

Correlated Noise of Fourier Reconstructed fMRI Data

Daniel B. Rowe^{1,2,*} and Raymond G. Hoffmann²
Department of Biophysics¹ and Division of Biostatistics²

Division of Biostatistics
Medical College of Wisconsin

Technical Report 51

June 2005

Division of Biostatistics
Medical College of Wisconsin
8701 Watertown Plank Road
Milwaukee, WI 53226
Phone: (414) 456-8280



Correlated Noise of Fourier Reconstructed fMRI Data

Daniel B. Rowe^{1,2*} and Raymond G. Hoffmann²

Department of Biophysics¹ and Division of Biostatistics²

Medical College of Wisconsin

Milwaukee, WI USA

Abstract

In magnetic resonance imaging, complex-valued measurements are acquired in time corresponding to measurements in spatial frequency or k -space. These measurements are “transformed” into a complex-valued image by an “image reconstruction” method. The most common image reconstruction method is the (inverse) Fourier transform. It is known that image voxels are spatially correlated. A property of the (inverse) Fourier transformation is that spatially uncorrelated k -space measurements yield spatially uncorrelated voxels and vice versa. Additionally, spatially correlated voxels result from spatially correlated k -space measurements. This paper examines the resulting correlation structure between voxels when Fourier reconstructing spatially correlated k -space observations and implications to fMRI results. A real-valued isomorphism for the complex-valued data is introduced, and an associated multivariate normal distribution. The signal and noise characteristics of both simulated and experimental phantom data are examined. It was found that autocorrelated observations along the spatial frequency trajectory within but not between the real and imaginary components in k -space produce voxels after Fourier reconstruction that have correlation both within and between real and imaginary components. One implication of these results is that one source of spatial correlation between voxels may be (temporally) autocorrelated observations in k -space.

1 Introduction

In magnetic resonance imaging, we aim to image the effective density of proton “spins” in a real-valued physical object. In magnetic resonance imaging (MRI), complex-valued measurements are acquired in spatial frequency space (usually two dimensional), also called k -space from the use of the k variables for its axes (k_x, k_y). These measurements are “transformed” into a complex-valued image by an “image reconstruction” method. The most common image reconstruction method is the inverse Fourier transform.

In MRI/fMRI, a set of differential equations (Bloch, 1946, Bloch et al., 1946) describes the time dependent behavior of the bulk magnetization in applied magnetic fields. By Faraday’s law of induction a voltage is induced in

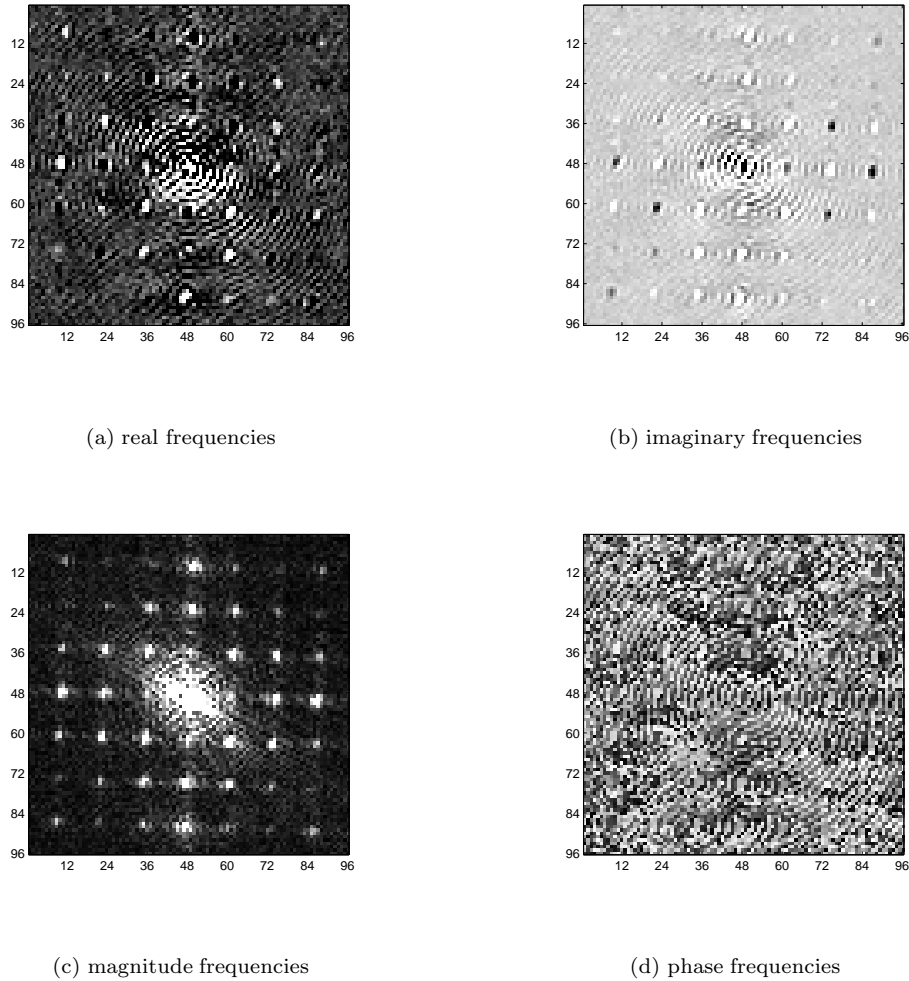
*Corresponding Author: Daniel B. Rowe, Department of Biophysics, Medical College of Wisconsin, 8701 Watertown Plank Road, Milwaukee, WI 53226, dbrowe@mcw.edu.

a receive coil that is placed near the sample. It is the voltage/signal in the wire $s(t)$ that we measure over time. By varying gradient magnetic fields in a particular way known as “Fourier encoding,” the argument of the signal $s(t)$ can be rewritten in terms of complex-valued spatial frequencies $(k_x(t), k_y(t))$ and given by

$$s(k_x, k_y) = \int \int \rho(x, y) e^{-i2\pi[k_x(t)x + k_y(t)y]} dx dy$$

where $\rho(x, y)$ is the effective proton spin density image, $k_x(t) = \frac{\gamma}{2\pi} \int_0^t G_x(t') dt'$, and $k_y(t) = \frac{\gamma}{2\pi} \int_0^t G_y(t') dt'$. For Hydrogen nuclei, $\gamma/(2\pi) = 42.58\text{MHz/T}$. Although $s(t)$ is real-valued and measured over time, we complex demodulate it and form $s(k_x, k_y)$ usually on or resampled to a Cartesian (k_x, k_y) grid. The above signal equation with

Figure 1: k -space measurements



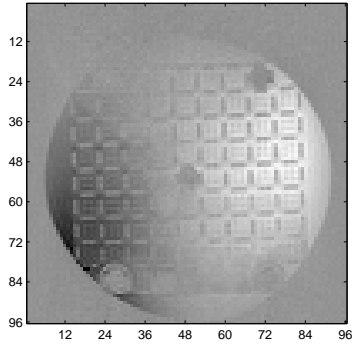
homogeneity assumptions characterizes the observed two dimensional complex-valued signal as the Fourier transform (FT) of the effective proton spin density (PSD). We measure the complex-valued spatial frequency spectrum (an example from phantom data to be described later is shown in Fig. 1) and perform an inverse Fourier transform (IFT) to obtain the effective proton spin density (an example of which as shown in Fig. 2). Mathematically this is

represented as

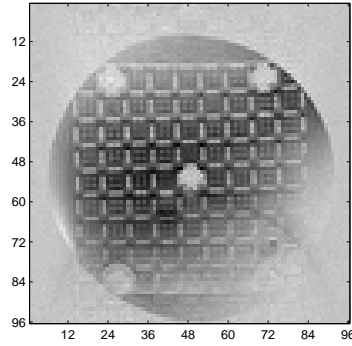
$$\underbrace{\rho(x, y)}_{Complex} = \int \int \underbrace{s(k_x, k_y)}_{Complex} e^{i2\pi(k_x x + k_y y)} dk_x dk_y .$$

This is done by taking successive measurements in time of a real-valued signal, a voltage in a wire. The time axis is transformed to the spatial frequency or k -space axis. This physical signal or voltage is real-valued, but it is “complex demodulated.”

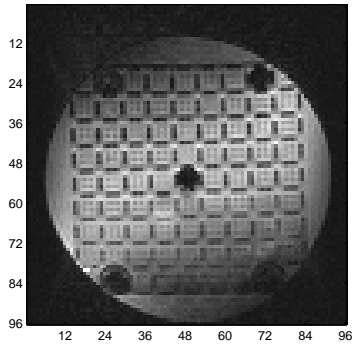
Figure 2: Fourier reconstructed images



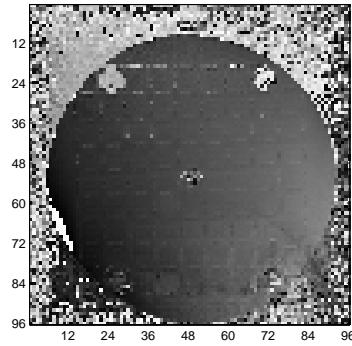
(a) real image



(b) imaginary image



(c) magnitude image



(d) phase image

In measuring the signal, each complex-valued point measurement is obtained by taking pairs of real-valued signal measurements where the first in the pair is multiplied by a cosine and the second by a sine to obtain real (in-phase) and imaginary (quadrature) parts. In taking the pairs of measurements, either one or two analog-to-digital (A-to-D) converters are utilized. If there is a single A-to-D converter, successive signal measurements are alternately multiplied by either a cosine or a sine to obtain real (in-phase) and imaginary (quadrature) parts. These two measurements are then shifted either half a step forward or backward to temporally align them. If there are two A-to-D converters,

two measurements, one from each A-to-D, are then taken at the same time with the first multiplied by a cosine and the second by a sine.

These discrete complex-valued measurements, when placed at their proper spatial frequency location, are the discrete FT of the PSD. A discrete IFT is applied to the discretely measured signal to “reconstruct” the PSD. The original object or PSD is real valued, but due to imperfections in the imaging process, a complex image of PSDs is produced (Haacke et al., 1999).

After Fourier (or non-Fourier) image reconstruction, each voxel contains a complex-valued time course of real and imaginary components of the measured PSD. It is known that image voxels are spatially correlated, as evidenced in magnitude-only fMRI data. A property of the (inverse) Fourier transformation is that spatially uncorrelated k -space measurements yield spatially uncorrelated voxels and vice versa. Additionally, spatially correlated voxels result from spatially correlated k -space measurements. The thrust of this paper is to examine the noise characteristics in k -space data and Fourier reconstructed images. Implications for fMRI will also be discussed. This will be done with both one and two dimensional images focusing a subset of the data in the central portion of k -space for a single axial slice.

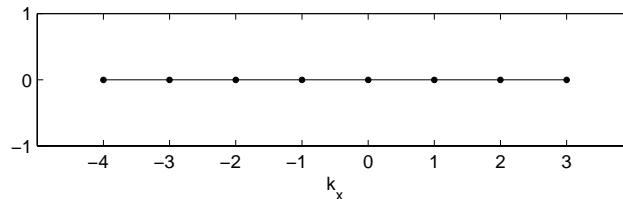
2 Models

In this section, the observed complex-valued signal over space is examined for a single time point image. The complex-valued (inverse) Fourier transformation commonly used for magnetic resonance (MR) image reconstruction of the observed complex-valued spatial frequencies is described. This is done for both a one dimensional image, where the characteristics are clearer, and for a two dimensional image.

2.1 One Dimension

Consider a one dimensional complex-valued MR image that is $1 \times p_x$ acquired from left to right. In a one dimensional echo planar MRI, complex-valued k -space measurements are taken in time but correspond to specific spatial frequencies on this $(k_x, k_y = 0)$ grid as in Fig. 3. Let $s_C = (s_{C1}, \dots, s_{Cp_x})'$ be a $p_x \times 1$ complex-valued vector

Figure 3: 1D k -space trajectory.



of one dimensional image spatial frequencies such that

$$\begin{matrix} s_C & = & s_{0C} & + & \epsilon_C \\ p_x \times 1 & & p_x \times 1 & & p_x \times 1 \end{matrix} \quad (2.1)$$

where s_{0C} is the true noiseless complex-valued vector of spatial frequencies and ϵ_C is the vector of complex-valued measurement error. The statistical properties of these measurements will be discussed in the next section. The measured complex valued signal can be represented as

$$\begin{aligned} s_C &= (s_{0R} + i s_{0I}) + (\epsilon_R + i \epsilon_I) \\ &= (s_{0R} + \epsilon_R) + i(s_{0I} + \epsilon_I) \end{aligned}$$

where i is the imaginary unit while s_{0R} , s_{0I} , ϵ_R and ϵ_I are real and imaginary vector valued parts of the true signal and measurement noise. Also let Ω_{Cx} be a $p_x \times p_x$ complex-valued matrix such as a Fourier matrix such that

$$\begin{array}{rcc} \Omega_{Cx} & = & \Omega_{Rx} + i \Omega_{Ix} \\ p_x \times p_x & & p_x \times p_x \quad p_x \times p_x \end{array}$$

where Ω_{Rx} and Ω_{Ix} are real and imaginary matrix valued parts. Then, the $p_x \times 1$ complex-valued (inverse) Fourier transformation ρ_C of s_C can be written (Strang, 1988) as the pre multiplication by the complex-valued Fourier matrix as

$$\begin{aligned} \rho_C &= \Omega_{Cx} * s_C \\ &= (\Omega_{Rx} + i \Omega_{Ix}) * [(s_{0R} + \epsilon_R) + i(s_{0I} + \epsilon_I)] \\ &= [\Omega_{Rx}(s_{0R} + \epsilon_R) - \Omega_{Ix}(s_{0I} + \epsilon_I)] + i[\Omega_{Rx}(s_{0I} + \epsilon_I) + \Omega_{Ix}(s_{0R} + \epsilon_R)] \\ &= [(\Omega_{Rx}s_{0R} - \Omega_{Ix}s_{0I}) + (\Omega_{Rx}\epsilon_R - \Omega_{Ix}\epsilon_I)] + i[(\Omega_{Rx}s_{0I} + \Omega_{Ix}s_{0R}) + (\Omega_{Rx}\epsilon_I + \Omega_{Ix}\epsilon_R)] \\ &= (\rho_{0R} + \eta_R) + i(\rho_{0I} + \eta_I) \\ &= \rho_R + i\rho_I \end{aligned}$$

where ρ_{0R} , ρ_{0I} , η_R , and η_I are real and imaginary vector valued parts of the Fourier transformed true signal (image) and transformed measurement noise. If Ω_{Cx} were a Fourier matrix, it is $[\Omega_{Cx}]_{jk} = \kappa(\omega^{jk})$ where $\kappa = 1$ and $\omega = \exp[-i2\pi(j-1)(k-1)/p_x]$ for the forward transformation while $\kappa = 1/p_x$ and $\omega = \exp[+i2\pi(j-1)(k-1)/p_x]$ for the inverse transformation, where $j, k = 1, \dots, p_x$.

This pre multiplication of a complex-valued vector by a complex-valued matrix can be equivalently represented with the $2p_x$ dimensional real-valued isomorphism

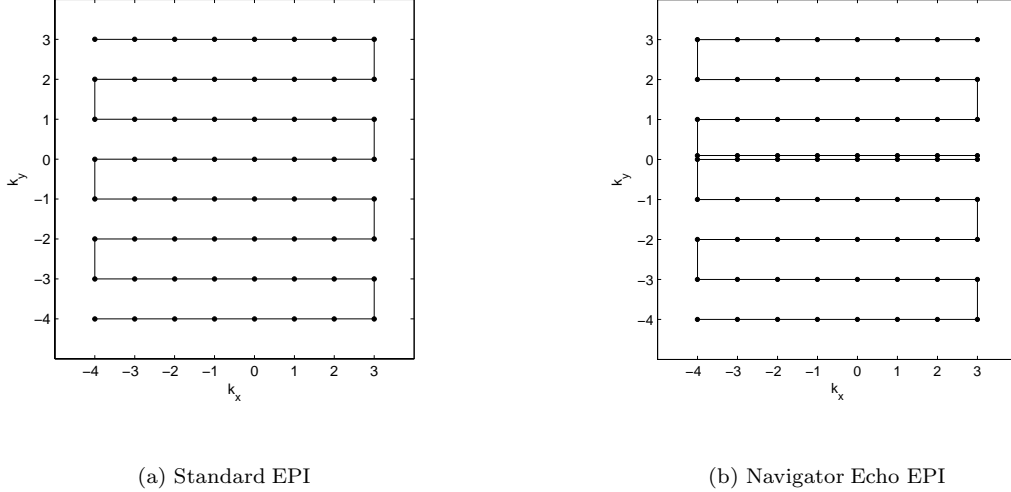
$$\begin{pmatrix} \rho \\ \rho_R \\ \rho_I \end{pmatrix} = \begin{pmatrix} \Omega_x \\ \Omega_{Rx} & -\Omega_{Ix} \\ \Omega_{Ix} & \Omega_{Rx} \end{pmatrix} * \begin{pmatrix} s \\ s_{0R} + \epsilon_R \\ s_{0I} + \epsilon_I \end{pmatrix}. \quad (2.2)$$

2.2 Two Dimensions

In a two dimensional echo planar MRI, two dimensional complex-valued k -space measurements are taken in time but correspond to specific spatial frequencies on a (k_x, k_y) grid. In a standard echo planar imaging (EPI) experiment, the measurements are taken in a ‘‘zig-zag’’ pattern. For example, with positive phase encode steps, the pattern starts at the bottom left of the grid with negative (k_x, k_y) values and moves from left to right, then right to left and so on, while going from bottom to top, as in Fig. 4a, which exemplifies an eight line image. A modification of this standard EPI k -space trajectory is to repeat the center line in the vertical k_y direction (pictorially separated) then

continue in a zig-zag pattern, as in Fig. 4b, which exemplifies an eight line image. This repeated central k_y line from the omission of a phase encode step allows for an adjustment to be performed to compensate for misalignment between odd and even lines of k -space that may cause Nyquist ghosting in the phase encode direction (Jesmanowicz et al., 1993; Jesmanowicz et al., 1995), which is vertical here. The left-right direction is called the frequency encode direction. After this correction, the second or repeated line through the center of k -space is discarded.

Figure 4: 2D EPI k -space trajectories.



Let S_C be a $p_y \times p_x$ complex-valued matrix of two dimensional image spatial frequencies such that

$$\begin{array}{ccccc}
 S_C & = & S_{0C} & + & E_C \\
 p_y \times p_x & & p_y \times p_x & & p_y \times p_x
 \end{array} \tag{2.3}$$

where S_{0C} is the true noiseless complex-valued matrix of spatial frequencies and E_C is the matrix of complex-valued measurement error. The statistical properties of these measurements will be discussed in the next section.

The measured complex valued signal can be represented as

$$\begin{aligned}
 S_C &= (S_{0R} + iS_{0I}) + (E_R + iE_I) \\
 &= (S_{0R} + E_R) + i(S_{0I} + E_I)
 \end{aligned}$$

where i is the imaginary unit while S_{0R} , S_{0I} , E_R and E_I are real and imaginary matrix valued parts of the true signal and measurement noise.

Let Ω_{C_x} and Ω_{C_y} be $p_x \times p_x$ and $p_y \times p_y$ complex-valued Fourier matrices such that

$$\begin{array}{ccccccc}
 \Omega_{C_y} & = & \Omega_{Ry} & + & i & \Omega_{Iy} & \text{and} & \Omega_{C_x} & = & \Omega_{Rx} & + & i & \Omega_{Ix} \\
 p_y \times p_y & & p_y \times p_y & & & p_y \times p_y & & p_x \times p_x & & p_x \times p_x & & & p_x \times p_x
 \end{array}$$

where Ω_{Ry} and Ω_{Rx} are real, and Ω_{Iy} Ω_{Ix} are imaginary matrix valued parts.

Then, the $p_y \times p_x$ complex-valued (inverse) Fourier transformation R_C of S_C can be written as

$$\begin{aligned}
R_C &= \Omega_{C_y} && S_C && \Omega'_{C_x} \\
&= (\Omega_{R_y} + i\Omega_{I_y}) && [(S_{0R} + E_R) + i(S_{0I} + E_I)] && (\Omega'_{R_x} + i\Omega'_{I_x}) \\
&= (\Omega_{R_y} + i\Omega_{I_y}) && \{[(S_{0R} + E_R)\Omega'_{R_x} - (S_{0I} + E_I)\Omega'_{I_x}] + i[(S_{0R} + E_R)\Omega'_{I_x} + (S_{0I} + E_I)\Omega'_{R_x}]\} \\
&= (R_{0R} + N_R) + && i(R_{0I} + N_I) \\
&= R_R + && iR_I
\end{aligned}$$

where

$$\begin{aligned}
R_{0R} &= (\Omega_{R_y}S_{0R}\Omega'_{R_x} - \Omega_{R_y}S_{0I}\Omega'_{I_x} - \Omega_{I_y}S_{0R}\Omega'_{I_x} - \Omega_{I_y}S_{0I}\Omega'_{R_x}) \\
N_R &= (\Omega_{R_y}E_R\Omega'_{R_x} - \Omega_{R_y}E_I\Omega'_{I_x} - \Omega_{I_y}E_R\Omega'_{I_x} - \Omega_{I_y}E_I\Omega'_{R_x}) \\
R_{0I} &= (\Omega_{R_y}S_{0R}\Omega'_{I_x} + \Omega_{R_y}S_{0I}\Omega'_{R_x} + \Omega_{I_y}S_{0R}\Omega'_{R_x} - \Omega_{I_y}S_{0I}\Omega'_{I_x}) \\
N_I &= (\Omega_{R_y}E_R\Omega'_{I_x} + \Omega_{R_y}E_I\Omega'_{R_x} + \Omega_{I_y}E_R\Omega'_{R_x} - \Omega_{I_y}E_I\Omega'_{I_x})
\end{aligned}$$

are real and imaginary matrix valued parts of the Fourier transformed true signal (image) and measurement noise. Each row in the curled bracket part of the expression for R_C is a one dimensional complex-valued transformation

$$S_C\Omega'_{C_x} = \begin{pmatrix} (\Omega_{C_x} s_{C1})' \\ \vdots \\ (\Omega_{C_x} s_{Cp_y})' \end{pmatrix} \quad (2.4)$$

as in the previous subsection where s'_{Cj} represents the j^{th} row in S_C that is p_x dimensional, $j = 1, \dots, p_y$. The complex matrices Ω_{C_y} and Ω_{C_x} can be Fourier matrices. This pre and post multiplication of a complex-valued matrix by complex-valued matrices could in principle be equivalently represented with a real-valued isomorphism but this is difficult to work with.

3 Statistics

As described in the previous section, data collected from a scientific experiment is never precisely known and thus contains both true signal and measurement error. Scientific measurement error is quantified with statistical distributions and inferences drawn. In most instances, real-valued measurements are taken and real-valued statistical distributions utilized. However, in MRI complex-valued measurements are taken and thus a complex-valued statistical distribution needs to be utilized. The data can be represented using a real-valued isomorphism and a multivariate normal distribution (Rowe, 2003). The real-valued isomorphism used here is very general and within this framework contains the particular isomorphism used to represent the complex-valued multivariate normal distribution (Wooding, 1956; Anderson et al., 1995) as briefly described in Appendix A . The transformation from complex-valued spatial frequency space to image space modifies properties of both the true signal and the measurement noise. The relationship between correlated complex-valued observations made in spatial frequency space and the modified correlation between Fourier transformed or reconstructed complex-valued observations in image space is examined.

3.1 One Dimension

Using the real-valued isomorphism in Eqn. 2.2, let the $2p_x$ dimensional vector $s = (s'_R, s'_I)'$ be multivariate normally distributed (Rowe, 2003) with mean and covariance matrix

$$s_0 = \begin{pmatrix} s_{0R} \\ s_{0I} \end{pmatrix} \quad \text{and} \quad \Lambda = \begin{pmatrix} \Lambda_{11} & \Lambda_{12} \\ \Lambda'_{12} & \Lambda_{22} \end{pmatrix}$$

Complex multivariate normal structure occurs when $\Lambda_{11} = \Lambda_{22} = \Psi$, $-\Lambda_{12} = \Upsilon$, and $\Lambda'_{12} = \Upsilon$. This isomorphism is more general and less restrictive than multivariate complex normal structure. By carrying out a multivariate transformation of variable with the real-valued isomorphism from s to ρ through $\rho = \Omega_x s$, the statistical distribution of ρ is also multivariate normally distributed but with mean ρ_0 given by

$$\begin{aligned} \begin{pmatrix} \rho_{0R} \\ \rho_{0I} \end{pmatrix} &= \begin{pmatrix} \Omega_{Rx} & -\Omega_{Ix} \\ \Omega_{Ix} & \Omega_{Rx} \end{pmatrix} \begin{pmatrix} s_{0R} \\ s_{0I} \end{pmatrix} \\ &= \begin{pmatrix} \Omega_{Rx}s_{0R} - \Omega_{Ix}s_{0I} \\ \Omega_{Rx}s_{0I} + \Omega_{Ix}s_{0R} \end{pmatrix} \end{aligned} \quad (3.1)$$

and covariance matrix $\Delta = \Omega_x \Lambda \Omega'_x$ given by

$$\begin{aligned} \Delta &= \begin{pmatrix} \Omega_{Rx} & -\Omega_{Ix} \\ \Omega_{Ix} & \Omega_{Rx} \end{pmatrix} \begin{pmatrix} \Lambda_{11} & \Lambda_{12} \\ \Lambda'_{12} & \Lambda_{22} \end{pmatrix} \begin{pmatrix} \Omega'_{Rx} & \Omega'_{Ix} \\ -\Omega'_{Ix} & \Omega'_{Rx} \end{pmatrix} \\ \Delta_{11} &= \Omega_{Rx}\Lambda_{11}\Omega'_{Rx} - \Omega_{Ix}\Lambda'_{12}\Omega'_{Rx} + \Omega_{Rx}(-\Lambda_{12})\Omega'_{Ix} + \Omega_{Ix}\Lambda_{22}\Omega'_{Ix} \\ \Delta_{22} &= \Omega_{Ix}\Lambda_{11}\Omega'_{Ix} + \Omega_{Rx}\Lambda'_{12}\Omega'_{Ix} - \Omega_{Ix}(-\Lambda_{12})\Omega'_{Rx} + \Omega_{Rx}\Lambda_{22}\Omega'_{Rx} \\ \Delta_{12} &= \Omega_{Rx}\Lambda_{11}\Omega'_{Ix} - \Omega_{Ix}\Lambda'_{12}\Omega'_{Ix} - \Omega_{Rx}(-\Lambda_{12})\Omega'_{Rx} - \Omega_{Ix}\Lambda_{22}\Omega'_{Rx} \\ \Delta_{21} &= \Delta'_{12} \end{aligned} \quad (3.2)$$

where Ω_x is of full rank if it is a Fourier matrix. Again, this isomorphism is more general and less restrictive than multivariate complex normal structure. In the multivariate complex normal case where $\Lambda_{11} = \Lambda_{22} = \Psi$, $-\Lambda_{12} = \Upsilon$, and $\Lambda'_{12} = \Upsilon$,

$$\begin{aligned} \Delta_{11} &= \Omega_{Rx}\Psi\Omega'_{Rx} - \Omega_{Ix}\Upsilon\Omega'_{Rx} + \Omega_{Rx}\Upsilon\Omega'_{Ix} + \Omega_{Ix}\Psi\Omega'_{Ix} \\ \Delta_{12} &= \Omega_{Rx}\Psi\Omega'_{Ix} - \Omega_{Ix}\Upsilon\Omega'_{Ix} - \Omega_{Rx}\Upsilon\Omega'_{Rx} - \Omega_{Ix}\Psi\Omega'_{Rx} \\ \Delta_{21} &= -\Delta_{12} \\ \Delta_{22} &= \Delta_{11} \end{aligned} \quad (3.3)$$

where Υ is a skew symmetric matrix, $\Upsilon' = -\Upsilon$.

It can readily be seen that if the measurement process that generates the data produces independent real and imaginary channels, $\Lambda_{12} = \Lambda'_{12} = 0$ but correlated within the real and imaginary channels, then after transformation the real and imaginary channels are correlated both between and within. It should be noted that if $\Upsilon = 0$ and $\Psi = \psi^2 I_{p_x}$, then $\Delta = \delta^2 I_2 \otimes I_{p_x}$ where $\delta = \psi^2/p_x$ for the inverse transformation and $\delta = \psi^2 p_x$ for the forward transformation.

The above specific multivariate complex normal structure could alternatively be developed utilizing the complex multivariate normal distribution as described in Appendix A. A property of the complex multivariate normal distribution is that if $s_C \sim N_C(s_{0C}, \Lambda_C)$, then $\rho_C = \Omega_{C_x} s_C$ is also complex normal distributed, $\rho_C \sim N_C(\Omega_{C_x} s_{0C}, \Omega_{C_x} \Lambda_C \Omega_{C_x}^H)$ where $\Lambda_C = \Psi + i\Upsilon$.

After image reconstruction, the usual procedure is to convert from real and imaginary images to magnitude and phase images. The phase is generally discarded in fMRI and magnitude-only time course data is analyzed. The conversion from real and imaginary images to magnitude and phase images is a nonlinear transformation and thus the joint distribution of the magnitude image observations is not straight forward. On an individual basis, the magnitude quantity in voxel j in each magnitude image is

$$m_j = \sqrt{(\rho_{0Rj} + \eta_{Rj})^2 + (\rho_{0Ij} + \eta_{Ij})^2}$$

and the vector $m = (m_1, \dots, m_{p_x})'$. It is well known (Rice, 1944; Gudbjartsson and Patz, 1995; Rowe and Logan, 2004) that m_j is Ricean distributed with parameters $a_j = \sqrt{\rho_{0Rj}^2 + \rho_{0Ij}^2}$ and Δ_{jj} as previously defined. The population correlation between Ricean distributed magnitude image observations will be examined through simulation in the next Section.

3.2 Two Dimensions

Similar to the one dimensional image case, let the real part stacked upon the imaginary part of each row of S_C , s_{Cj} be denoted by $s_j = (s'_{Rj}, s'_{Ij})'$ and be normally distributed with mean $s_{0j} = (s'_{0Rj}, s'_{0Ij})'$ and covariance matrix Λ_j . Define a real-valued isomorphism for each row of the complex-valued matrix to be

$$S = \begin{pmatrix} s'_1 \\ \vdots \\ s'_{p_y} \end{pmatrix}.$$

Each row of S can be post multiplied by Ω'_x and the resulting row is the transpose of the result for the one dimensional case given above. Reform a complex matrix then another real-valued isomorphism for the columns so that each of the resulting columns are pre multiplied by Ω_y to produce R .

As previously described, the observations can be represented with a real-valued isomorphism. Note that if each of the rows j of the two dimensional image are specified to be uncorrelated and normally distributed with mean s_{0j} and covariance matrix Λ_j , then the vector formed by stacking the rows is

$$\begin{pmatrix} s_1 \\ \vdots \\ s_{p_y} \end{pmatrix} \sim N \left(\begin{pmatrix} s_{01} \\ \vdots \\ s_{0p_y} \end{pmatrix}, \begin{pmatrix} \Lambda_1 & & 0 \\ & \ddots & \\ 0 & & \Lambda_{p_y} \end{pmatrix} \right)$$

the partial transformation along the x dimension can be written as

$$\begin{pmatrix} Q'_{R1}, Q'_{I1} \\ \vdots \\ Q'_{Rp_y}, Q'_{Ip_y} \end{pmatrix} = \begin{pmatrix} s'_{R1}, s'_{I1} \\ \vdots \\ s'_{Rp_y}, s'_{Ip_y} \end{pmatrix} \begin{pmatrix} \Omega'_{Rx} & \Omega'_{Ix} \\ -\Omega'_{Ix} & \Omega'_{Rx} \end{pmatrix}$$

then this is

$$\begin{pmatrix} Q_1 \\ \vdots \\ Q_{p_y} \end{pmatrix} \sim N \left(\begin{pmatrix} Q_{01} \\ \vdots \\ Q_{0p_y} \end{pmatrix}, \begin{pmatrix} \Delta_1 & & 0 \\ & \ddots & \\ 0 & & \Delta_{p_y} \end{pmatrix} \right)$$

where $Q_1 = (Q'_{R1}, Q'_{I1})' = s_1 \Omega'_x$, $Q_{01} = (Q'_{0R1}, Q'_{0I1})' = s_{01} \Omega'_x$, and $\Delta_j = \Omega_x \Lambda_j \Omega'_x$. Then the isomorphism

$$\begin{pmatrix} R'_{R1} \\ \vdots \\ R'_{Rp_y} \\ R'_{I1} \\ \vdots \\ R'_{Ip_y} \end{pmatrix} = \begin{pmatrix} \Omega_{Ry} & -\Omega_{Iy} \\ \Omega_{Iy} & \Omega_{Ry} \end{pmatrix} \begin{pmatrix} Q'_{R1} \\ \vdots \\ Q'_{Rp_y} \\ Q'_{I1} \\ \vdots \\ Q'_{Ip_y} \end{pmatrix}$$

where

$$\begin{pmatrix} Q_{R1} \\ \vdots \\ Q_{Rp_y} \\ Q_{I1} \\ \vdots \\ Q_{Ip_y} \end{pmatrix} \sim N \left(\begin{pmatrix} Q_{0R1} \\ \vdots \\ Q_{0Rp_y} \\ Q_{0I1} \\ \vdots \\ Q_{0Ip_y} \end{pmatrix}, \begin{pmatrix} \Delta_{1RR} & 0 & \Delta_{1RI} & 0 \\ & \ddots & & \\ 0 & \Delta_{p_y RR} & 0 & \Delta_{p_y RI} \\ \Delta_{1IR} & 0 & \Delta_{1II} & 0 \\ & \ddots & & \\ 0 & \Delta_{p_y IR} & 0 & \Delta_{p_y II} \end{pmatrix} \right)$$

with the matrix Δ_j partitioned into four blocks the upper left denoted RR the upper right denoted RI , the lower left IR and the lower right II . One could write down the pattern for the covariance matrix for the transformed data.

In terms of complex-valued matrices, the mean of the transformed variables can be written as

$$\begin{aligned} R_0 &= \Omega_y S_{0C} \Omega'_x \\ &= (\Omega_{yR} + i\Omega_{yI})(S_{0R} + iS_{0I})(\Omega'_{xR} + i\Omega'_{xI}) \\ &= R_{0R} + iR_{0I} \end{aligned}$$

as previously defined but the covariance of the transformed observations is nontrivial. The correlation structure of the two dimensional transformed data will be examined through rigorous simulation.

Again, after image reconstruction, the usual procedure is to convert from real and imaginary images to magnitude and phase images. The phase is generally discarded in fMRI and magnitude-only time course data is analyzed. The conversion from real and imaginary images to magnitude and phase images is a nonlinear transformation and thus

the joint distribution of the magnitude-only image quantities is not straight forward. On an individual basis, each magnitude image observation is

$$M_{jk} = \sqrt{(R_{0Rjk} + N_{Rjk})^2 + (R_{0Ijk} + N_{Ijk})^2}$$

and the matrix M with j, k th element M_{jk} formed. It is well known (Rice, 1944; Gudbjartsson and Patz, 1995; Rowe and Logan, 2004) that M_{jk} is Ricean distributed with parameter $a_{jk} = \sqrt{R_{0Rjk}^2 + R_{0Ijk}^2}$ as previously defined. The population correlation between Ricean distributed magnitude-only image quantities will be examined through simulation in the next Section.

4 Simulated Data

To illustrate the statistical properties of the transformed data, simulations were performed under known conditions. This will precisely characterize the distribution of the transformed observations. To illustrate the methods, simulations were carried out for the same dimensions for both the one and two dimensional image cases. All computations for both simulated and real data utilized Matlab (The Mathworks, Natick, MA, USA).

4.1 One Dimension

Although explicit analytical expressions exist for the mean and variance of the complex-valued transformed data given the mean and variance of the underlying true population distribution, simulations were carried out to verify the analytic results and obtain additional magnitude-only results. Data was generated to mimic a one dimensional magnetic resonance (MR) imaging experiment. Although this simulation is a mathematical ideal and possibly unrealistic, its results are useful in understanding the properties of the described methodology. Random complex-valued error vectors of dimension p_x were generated in the form of the real-valued isomorphism. Random error vectors of dimension $2p_x$ for the p_x real observations stacked upon the p_x imaginary observations denoted by s_1, \dots, s_L were generated from a normal distribution with mean s_0 and covariance $I_2 \times \Psi$. Without loss of generality, $s_0 = 0$ Ψ was taken to be a unit variance AR(1) correlation matrix with $(i, j)^{th}$ element $\rho^{|i-j|}$ where $\rho = 0.75$. The number of randomly generated vectors was selected to be $L = 10^7$.

Values of p_x were chosen to be 8, 32, 64, and 96. The corresponding correlation matrices from the L randomly generated vectors were computed as displayed in Figs. 5a, b and 6a, b. These correlation matrices matched the theoretical population correlation matrices from which they were generated. Note that the real and imaginary parts of the randomly generated data are statistically independent as seen in Figs. 5a, b and 6a, b. Further, each random vector for every p_x value was pre multiplied by the appropriate inverse Fourier transform matrix Ω given in Eqn. 2.2. The correlation matrices of the transformed vectors were computed as displayed in Figs. 5c, d and 6c, d. These correlation matrices matched the theoretical population correlation matrices from Eqn. 3.2. Note that the real and imaginary parts of the transformed data are correlated as seen in Figs. 5c, d and 6c, d. Further, since an analytic expression for the theoretical covariance or correlation matrix for magnitude-only quantities can not be found, the

L vectors containing real and imaginary observations of dimension $2p_x$ were converted to L vectors of dimension p_x containing magnitude-only quantities. The correlation matrices of the magnitude-only vectors was computed as displayed in Figs. 5e, f and 6e, f. Note that the magnitude-only quantities are nearly uncorrelated as seen in Figs. 5e and f while uncorrelated as seen in Figs. 6e and f.

It should also be noted that the simulated data was generated with population multivariate complex covariance structure and thus the transformed data also has complex multivariate normal covariance structure.

4.2 Two Dimensions

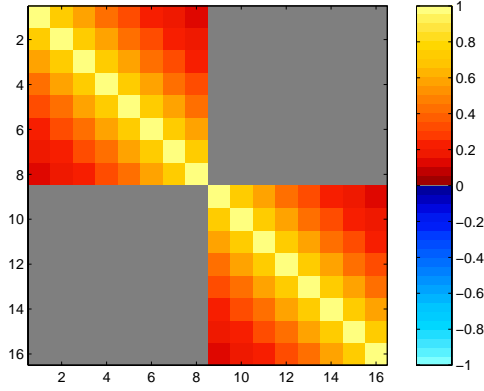
As previously noted, a simple closed form analytic expression for the correlation of real and imaginary parts of a transformed two dimensional image is not known. Data was generated to mimic a two dimensional magnetic resonance (MR) imaging experiment. Random complex-valued error matrices of dimension $p_y \times p_x$ were generated and denoted by S_1, \dots, S_L . The real and imaginary parts of each row along the EPI trajectory of Fig. 4b were generated from a normal distribution with mean S_0 and covariance $I_2 \otimes \Psi$. Voxels were ordered and oriented consistent with the path along a row either from left to right or right to left. Without loss of generality, $S_0 = 0$ and Ψ was taken to be the same as in the one dimensional case above. The number of randomly generated matrices was selected to be $L = 10^7$.

Values of $p_y = p_x$ were chosen to be 8 and 32. Results for 64 and 96 are not included for brevity and low information content but their pattern can be seen by generalizing the results of 8 and 32. Voxels are ordered in two ways when computing the correlation matrices. First following the zig-zag EPI path as in Fig. 4b and second by simply vectorizing (VEC) the voxels or ordering the voxels from top to bottom from left to right. In the VEC ordering of voxels, the correlation is spread out and the pattern lost. The sample correlation matrix from a finite number of observations is much noisier and when the VEC ordering is followed the correlations are more difficult to discern. The corresponding correlation matrices from the L randomly generated matrices were computed as displayed in Figs. 7a,b and 8a,b for the EPI and VEC paths. These correlation matrices matched the theoretical population correlation matrices from which they were generated. Note that the real and imaginary parts of the randomly generated data are statistically independent as seen in Figs. 7a,b and 8a,b. Further, each random complex-valued matrix for every $p_y = p_x$ value was pre and post multiplied by the appropriate inverse Fourier transform matrices Ω_{C_y} and Ω'_{C_x} given in Eqn. 2.2. The correlation matrices of the transformed data was computed as displayed in Figs. 7c,d and 8c,d. Since a simple closed form analytic expression for the theoretical covariance or correlation matrix for the transformed data matrices can not be simply found, the L data matrices containing $p_y p_x$ real and $p_y p_x$ imaginary observations were converted to L vectors of dimension $2p_y p_x$. This was done for both of the trajectory orderings of voxels. Note that the real and imaginary parts of the transformed data are correlated as seen in Figs. 7c,d and 8c,d. Further, since a simple closed form analytic expression for the theoretical covariance or correlation matrix for magnitude-only quantities can not be found, the L matrices of dimension $p_y = p_x$ containing real and imaginary observations were converted to L matrices of dimension $p_y \times p_x$ containing magnitude-only quantities. The correlation matrices of the magnitude-only data matrices was computed as displayed in Figs. 7e, f and 8e,f. Note that the magnitude-only

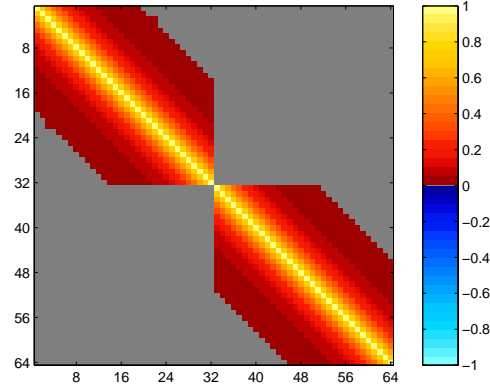
quantities are nearly uncorrelated as seen in Figs. 7e,f and 8g,h. Further note that the VEC ordering of the voxels spreads out the correlated voxels for the population correlation matrices as pictorially presented and thus in larger dimensions hides the pattern which may be further obfuscated in noisy sample correlation images.

Again, it should also be noted that the simulated data was generated with population multivariate complex covariance structure and thus the transformed data also has complex multivariate normal covariance structure.

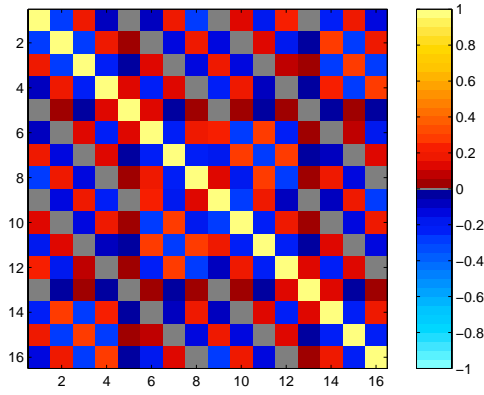
Figure 5: Correlation maps $\varrho = 0.75$, $L = 10^7$.



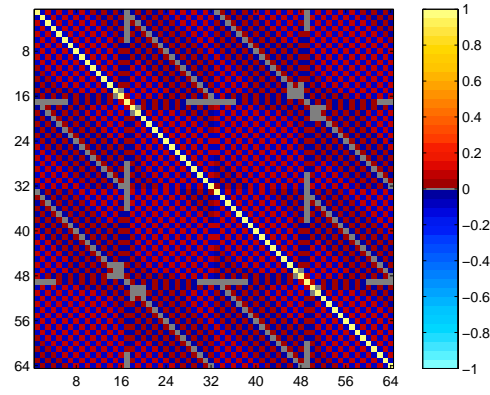
(a) $\text{Corr}(s(k_x), s(k_x))$, $p_x = 8$



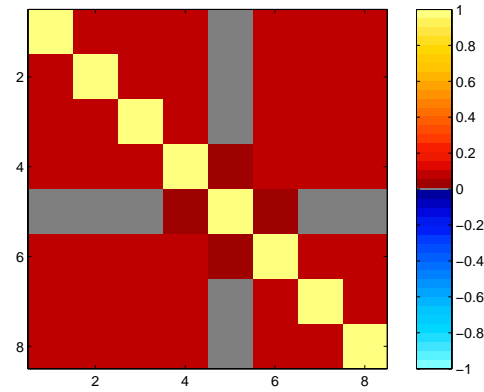
(b) $\text{Corr}(s(k_x), s(k_x))$, $p_x = 32$



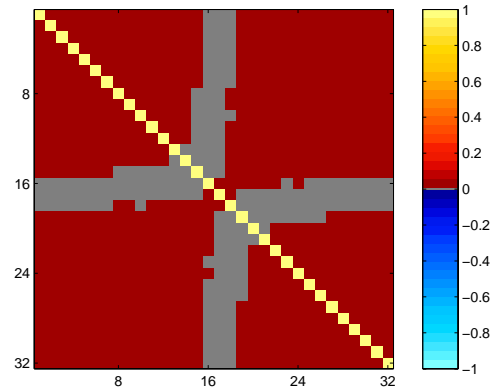
(c) $\text{Corr}(\rho(x), \rho(x))$, $p_x = 8$



(d) $\text{Corr}(\rho(x), \rho(x))$, $p_x = 32$

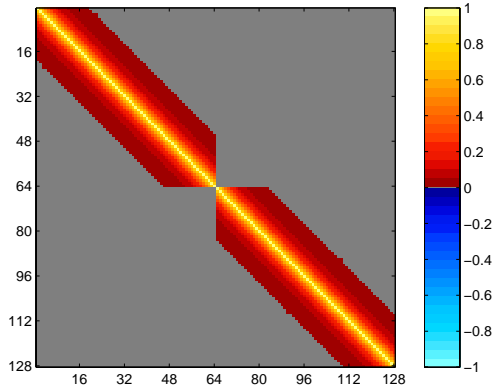


(e) $\text{Corr}(m(x), m(x))$, $p_x = 8$

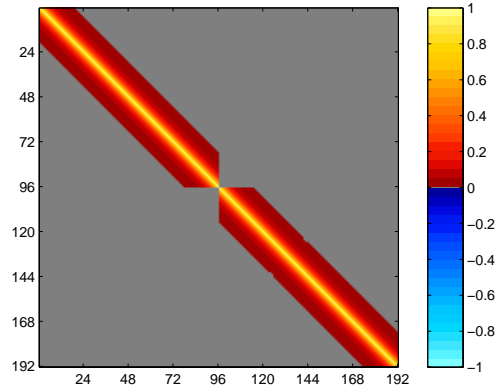


(f) $\text{Corr}(m(x), m(x))$, $p_x = 32$

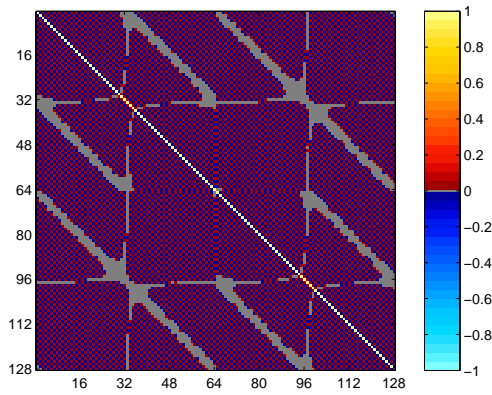
Figure 6: Correlation maps $\varrho = 0.75$, $L = 10^7$.



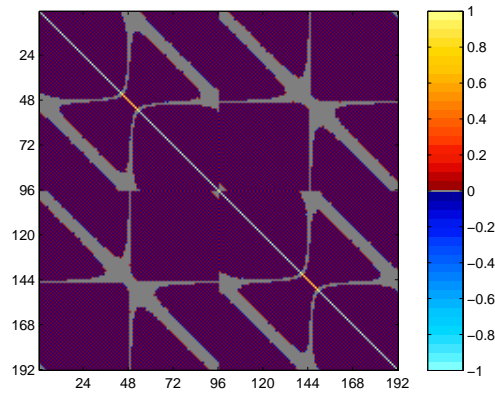
(a) $\text{Corr}(s(k_x), s(k_x))$, $p_x = 64$



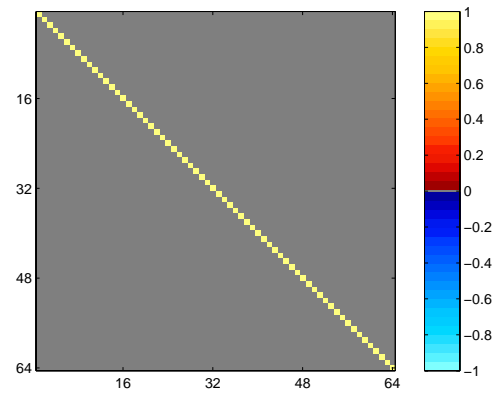
(b) $\text{Corr}(s(k_x), s(k_x))$, $p_x = 96$



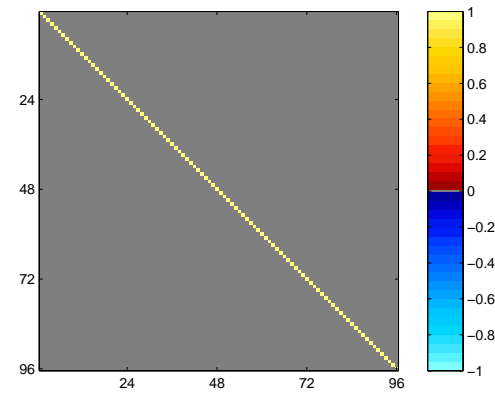
(c) $\text{Corr}(\rho(x), \rho(x))$, $p_x = 64$



(d) $\text{Corr}(\rho(x), \rho(x))$, $p_x = 96$

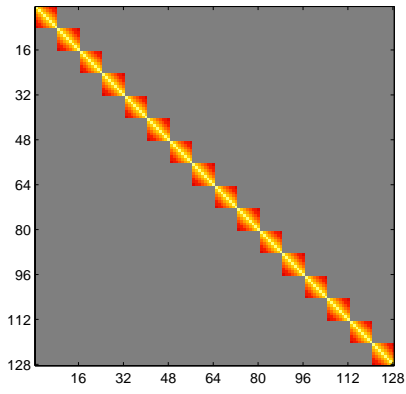


(e) $\text{Corr}(m(x), m(x))$, $p_x = 64$

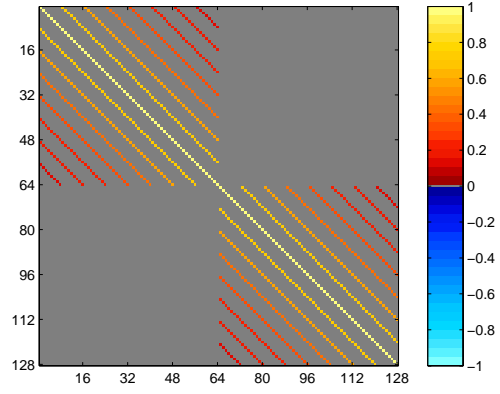


(f) $\text{Corr}(m(x), m(x))$, $p_x = 96$

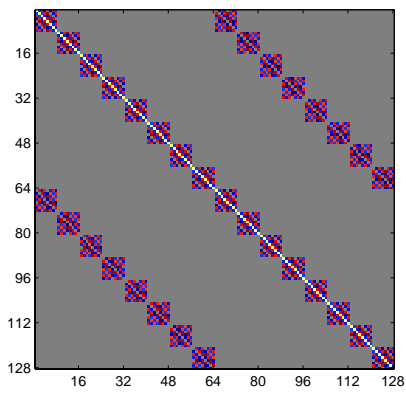
Figure 7: Correlation maps $p_y = p_x = 8$, $\rho = 0.75$, $L = 10^7$.



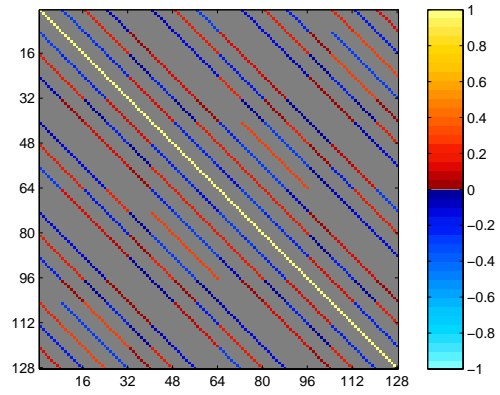
(a) $Corr(EPI(S), EPI(S))$



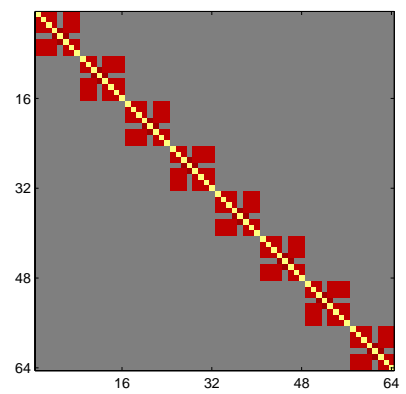
(b) $Corr(VEC(S), VEC(S))$



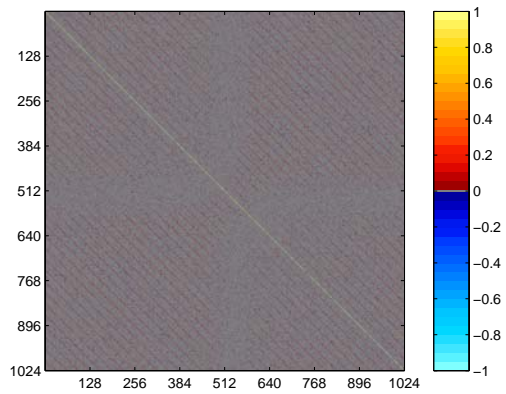
(c) $Corr(EPI(R), EPI(R))$



(d) $Corr(VEC(R), VEC(R))$

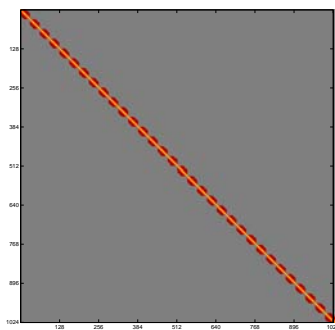


(e) $Corr(EPI(M), EPI(M))$

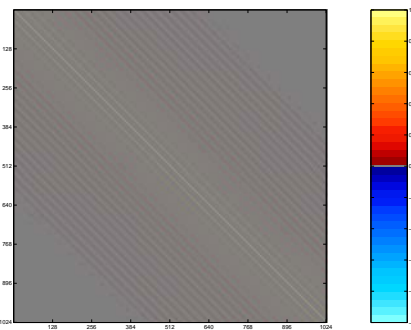


(f) $Corr(VEC(M), VEC(M))$

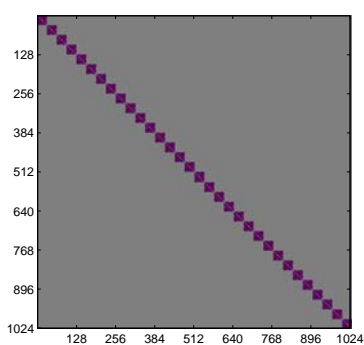
Figure 8: Correlation maps $p_y = p_x = 32$, $\varrho = 0.75$, $L = 10^7$.



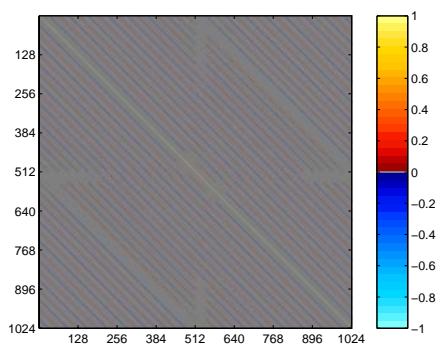
(a) $Corr(EPI(S_R), EPI(S_R))$



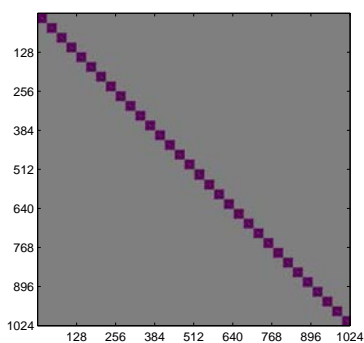
(b) $Corr(VEC(S_R), VEC(S_R))$



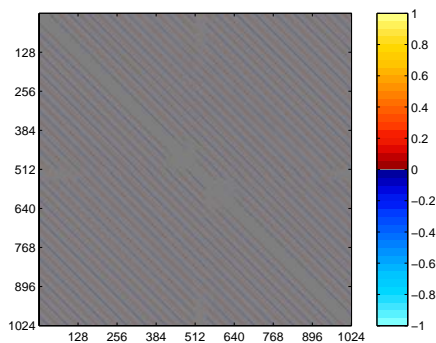
(c) $Corr(EPI(R_R), EPI(R_R))$



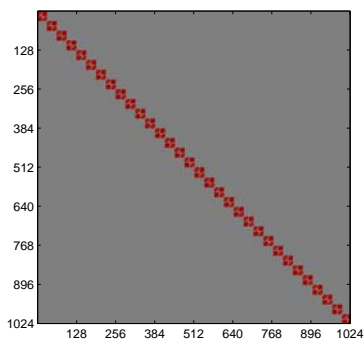
(d) $Corr(VEC(R_R), VEC(R_R))$



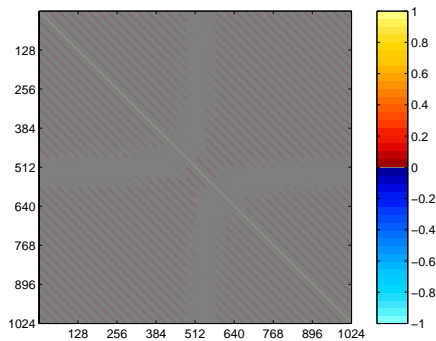
(e) $Corr(EPI(R_R), EPI(R_I))$



(f) $Corr(EPI(R_R), EPI(R_I))$



(g) $Corr(EPI(M), EPI(M))$



(h) $Corr(VEC(M), VEC(M))$

5 Experimental Data

To illustrate the properties of transformed data from actual biological experiments under known conditions without physiologically induced correlations, phantom data was acquired. An fMRI experiment was performed on a phantom containing aqueous cupric sulfate (CuSO_4) and a plastic grid. Scanning used a Bruker Medspec 3T/60cm scanner, where 10 axial slices of 96×96 were acquired with a field of view of 19.2cm. The dimension of each voxel was $2 \times 2 \times 2$ in mm. A single shot full k -space gradient echo EPI pulse sequences with FA= 90° , TE= 80ms, TR= 2000ms, and 330 time points was used. Within each of the acquired slices, data collection followed the EPI trajectory in Fig. 4b which started at the at the bottom left, then to the right, and up one line with a positive phase encode step then left and up with another phase encode step. This process was repeated until the Cartesian grid was completed. A repetition of the central k_y line or navigator echo of the center line as in Fig. 4b was performed by omitting a phase encode step. This allows for an adjustment to be performed to compensate for misalignment between odd and even lines of k -space that may cause Nyquist ghosting in the phase encode direction (Jesmanowicz et al., 1993; Jesmanowicz et al., 1995) which is vertical here. In the turn around of moving from left to right (or right to left), 32 turn around points were acquired and discarded after alignment.

A single axial slice is examined here, and the data reduced to $n = 256$ time points by omitting the first ten time points which allows for signal equilibration and the remaining points. This was performed to reduce the number of time points to a typical value so that these results may be translated to other experiments.

5.1 One Dimension

To demonstrate the aforementioned methodology in a single dimension, the center of the central line of k -space was utilized with voxels ordered from left to right of varying dimension p_x . Values of p_x were chosen to be 8, 32, 64, and 96. Since observed correlation matrices are noisier than population correlation matrices derived by a very large number of simulations, the neutral gray color band around zero was expanded to ± 0.05 . The corresponding sample correlation matrices from the $n = 256$ acquired vectors were computed as displayed in Figs. 9a, b and 10a, b. Note that the real and imaginary parts of the acquired data are correlated as seen in Figs. 9a,b and 10a,b. Further, each acquired vector for every p_x was pre multiplied by the appropriate inverse Fourier transform matrix Ω_x given in Eqn. 2.2. The sample correlation matrices of the transformed vectors was computed as displayed in Figs. 9c, d and 10c, d. Note that the real and imaginary parts of the transformed data are “strongly” correlated as seen in Figs. 9c,d and 10c, d. Further, the n vectors containing real and imaginary observations of dimension $2p_x$ were converted to n vectors of dimension p_x containing magnitude-only quantities. The sample correlation matrices of the magnitude-only vectors was computed as displayed in Figs. 9e,f and 10e,f. Note that the magnitude-only quantities are also “strongly” correlated as seen in Figs. 9e,f and Figs. 10e,f.

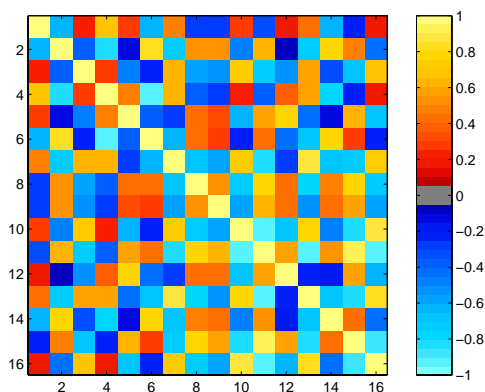
It should also be noted that the experimental data does not have multivariate complex covariance structure and thus the transformed data also does not have complex multivariate normal covariance structure.

5.2 Two Dimensions

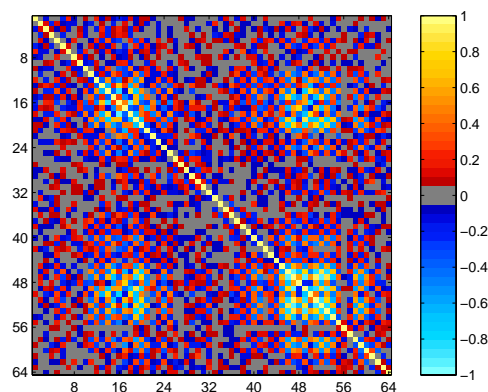
To further describe the above methodology, the central square of k -space of dimension $p_y \times p_x$ was utilized with voxels ordered and oriented as in the EPI navigator echo trajectory. Values of $p_y = p_x$ were chosen to be 8, 16, 32, and 64. The 96 dimensional results are not included as they are extremely difficult to obtain due to memory limitations and their information content is predicted to be low. Since observed correlation matrices are noisier than population correlation matrices derived by a very large number of simulations, the neutral gray color band around zero was expanded to ± 0.05 . The corresponding sample correlation matrices from the n acquired data matrices were computed as displayed in Figs. 11a,b - 13a,b and 15a,b for the EPI and VEC paths. Note that the real and imaginary parts of the observed data are statistically correlated as seen in Figs. 11a,b - 13a,b and 15a,b. Further, each acquired complex-valued matrix for every $p_y = p_x$ was pre and post multiplied by the appropriate inverse Fourier transform matrices Ω_{C_y} and Ω'_{C_x} given in Eqn. 2.2. The n transformed data matrices containing $p_y p_x$ real and $p_y p_x$ imaginary observations were converted to n vectors of dimension $2p_y p_x$. The sample correlation matrices of the transformed data was computed as displayed in Figs. 11c,d - 12c,d, 14a - f and 16a - f. This was done for both of the trajectory orderings of voxels. Note that the real and imaginary parts of the transformed data are correlated as seen in Figs. 11c,d - 12c,d, 14a - f and 16a - f. The n matrices of dimension $p_y = p_x$ containing real and imaginary observations were converted to n matrices of dimension $p_y \times p_x$ containing magnitude-only quantities. The sample correlation matrices of the magnitude-only data matrices was computed as displayed in Figs. 11e,f, 12e,f and 14g,h and 16g,h. Note that the magnitude-only quantities are correlated as seen in Figs. 11e,f, 12e,f and 14g,h and 16g,h.

Again, it should also be noted that the experimental data does not have multivariate complex covariance structure and thus the transformed data also does not have complex multivariate normal covariance structure.

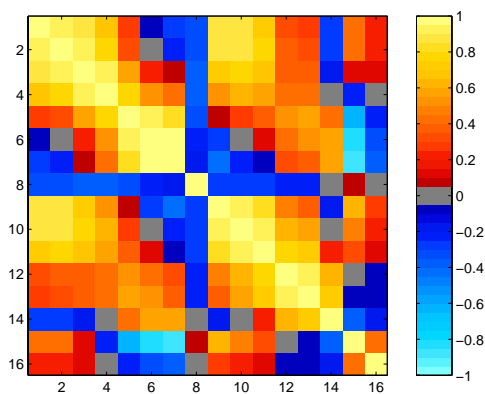
Figure 9: Correlation maps $\rho = Real$, $n = 256$.



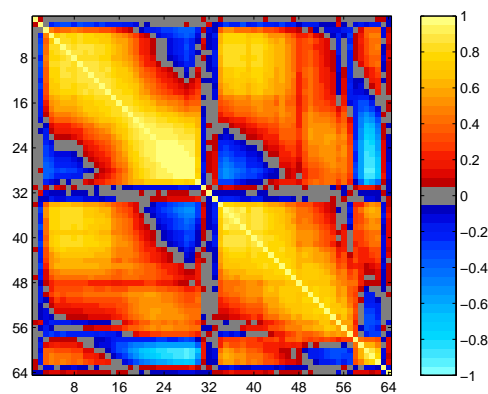
(a) $Corr(s(k_x), s(k_x))$, $p_x = 8$



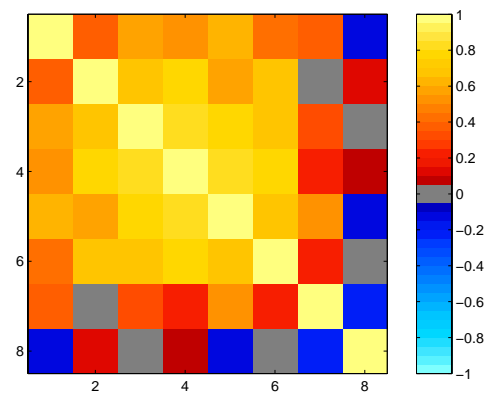
(b) $Corr(s(k_x), s(k_x))$, $p_x = 32$



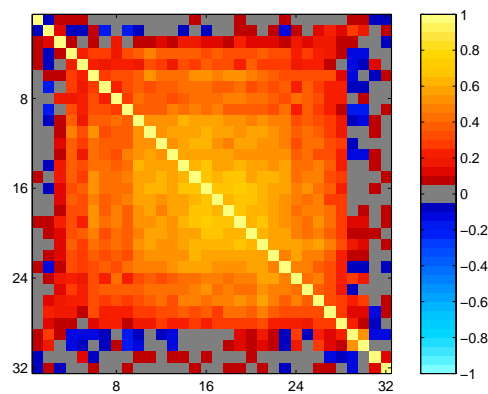
(c) $Corr(\rho(x), \rho(x))$, $p_x = 8$



(d) $Corr(\rho(x), \rho(x))$, $p_x = 32$

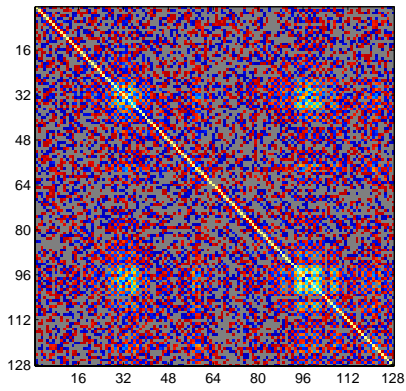


(e) $Corr(m(x), m(x))$, $p_x = 8$

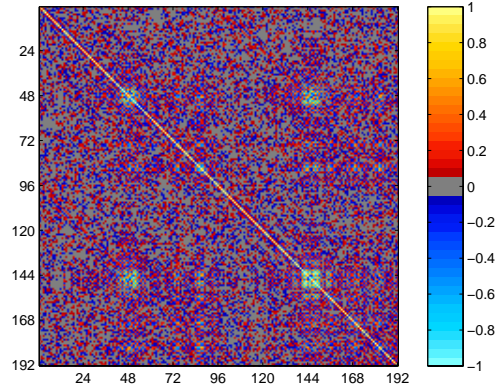


(f) $Corr(m(x), m(x))$, $p_x = 32$

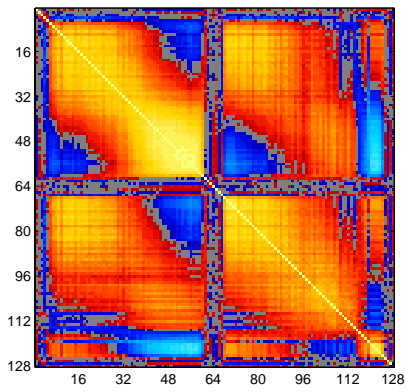
Figure 10: Correlation maps $\rho = \text{Real}$, $n = 256$.



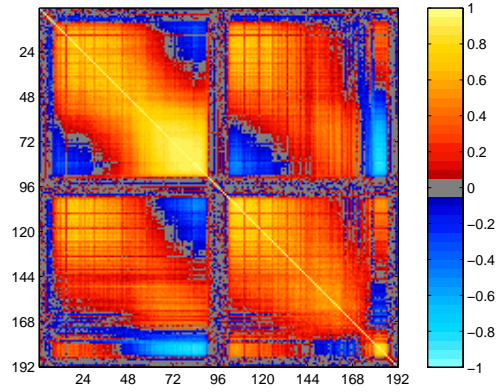
(a) $\text{Corr}(s(k_x), s(k_x))$, $p_x = 64$



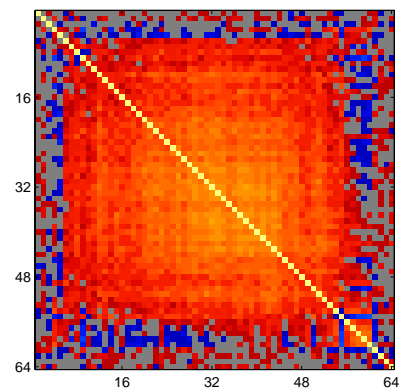
(b) $\text{Corr}(s(k_x), s(k_x))$, $p_x = 96$



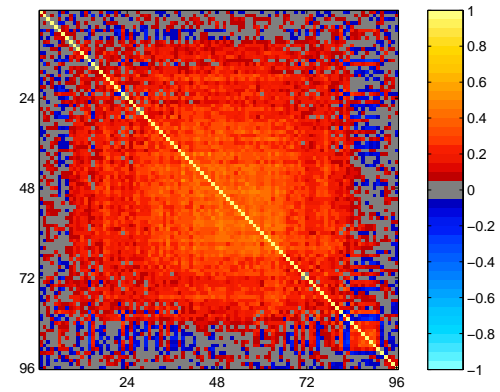
(c) $\text{Corr}(\rho(x), \rho(x))$, $p_x = 64$



(d) $\text{Corr}(\rho(x), \rho(x))$, $p_x = 96$

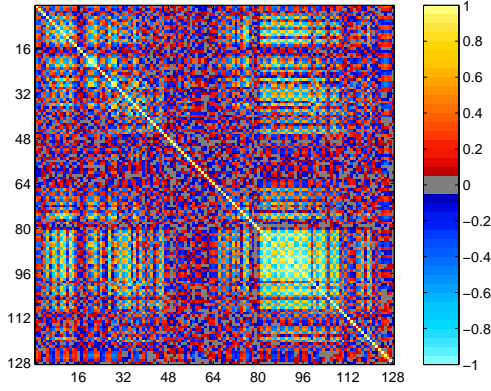


(e) $\text{Corr}(m(x), m(x))$, $p_x = 64$

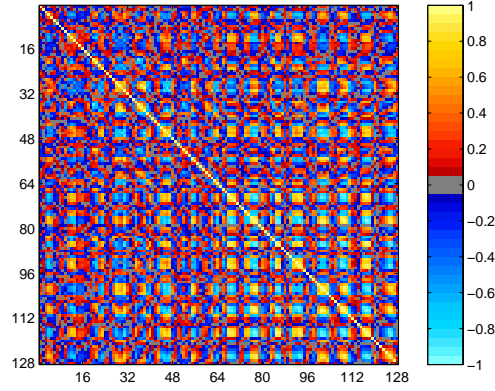


(f) $\text{Corr}(m(x), m(x))$, $p_x = 96$

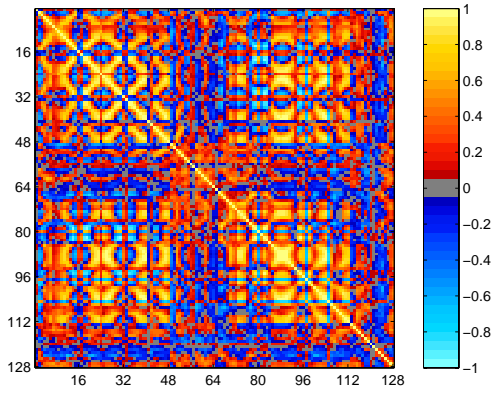
Figure 11: Correlation maps $p_y = p_x = 8$ $\rho = Real$, $n = 256$.



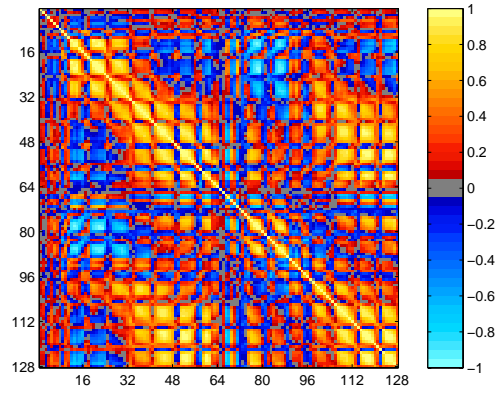
(a) $Corr(EPI(S), EPI(S))$



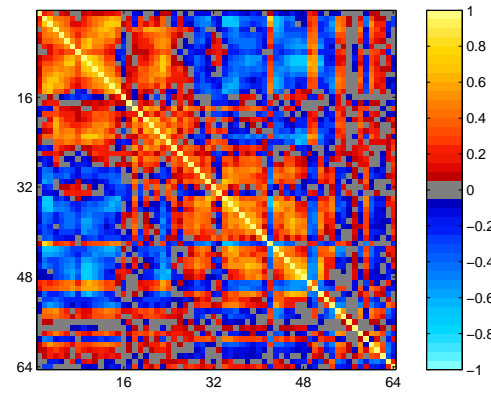
(b) $Corr(VEC(S), VEC(S))$



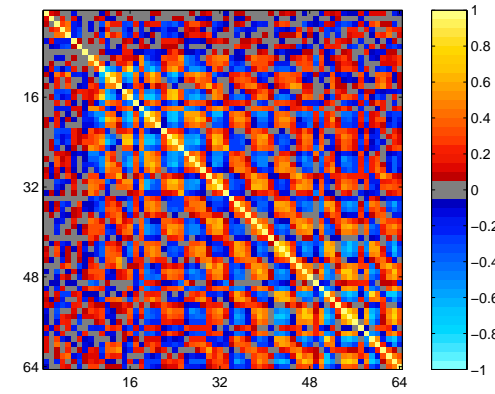
(c) $Corr(EPI(R), EPI(R))$



(d) $Corr(VEC(R), VEC(R))$

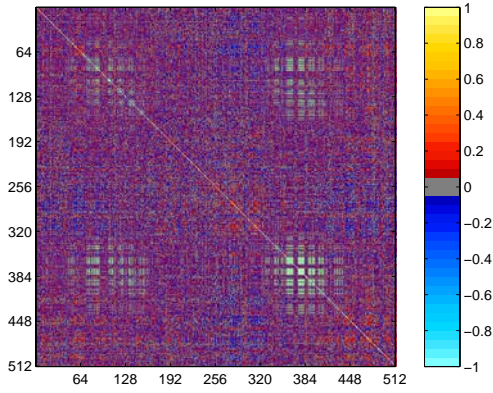


(e) $Corr(EPI(M), EPI(M))$

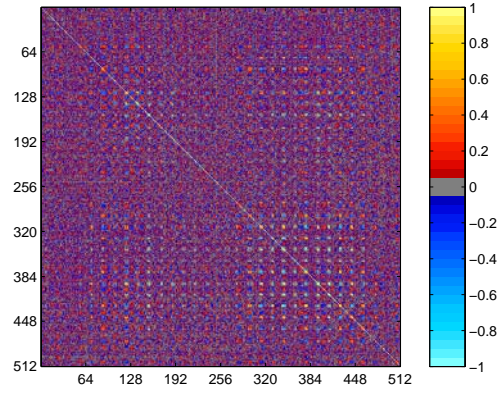


(f) $Corr(VEC(M), VEC(M))$

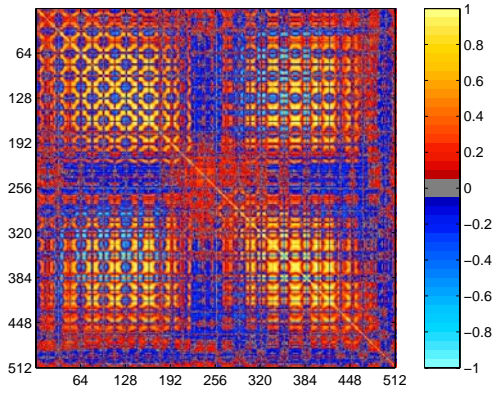
Figure 12: Correlation maps $p_y = p_x = 16$ $\rho = Real$, $n = 256$.



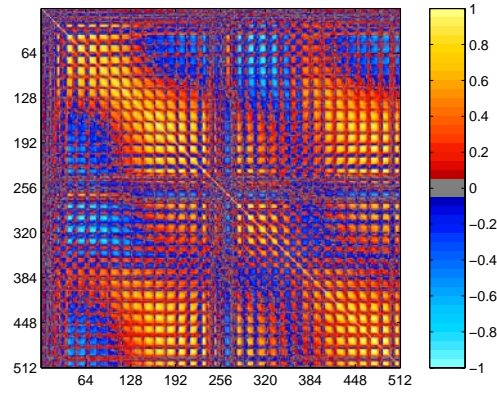
(a) $Corr(EPI(S), EPI(S))$



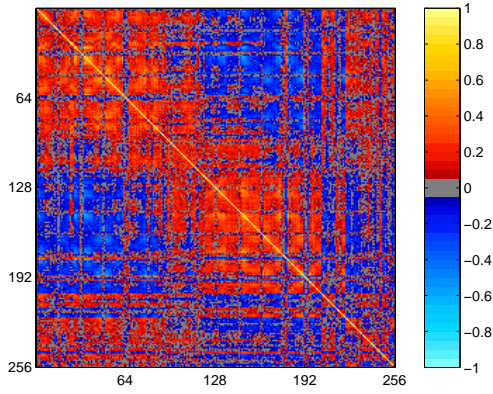
(b) $Corr(VEC(S), VEC(S))$



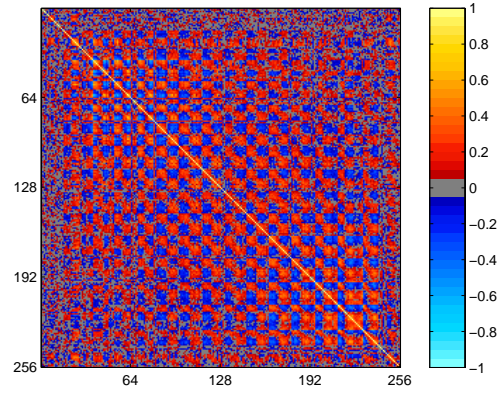
(c) $Corr(EPI(R), EPI(R))$



(d) $Corr(VEC(R), VEC(R))$

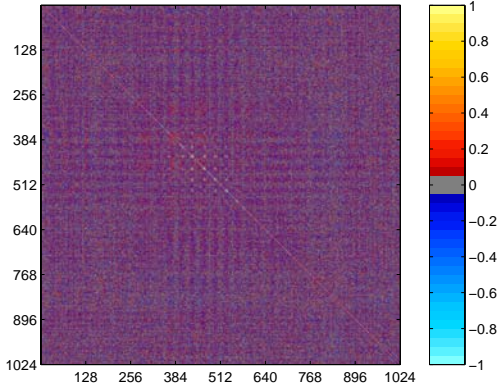


(e) $corr(EPI(M), EPI(M))$

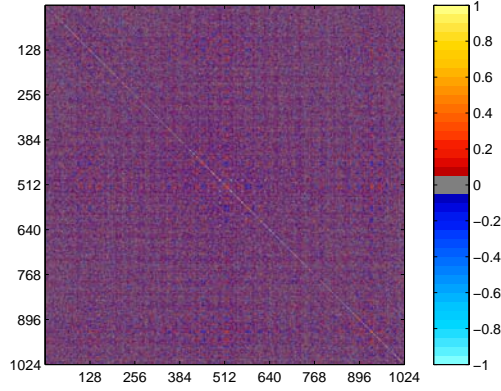


(f) $Corr(VEC(M), VEC(M))$

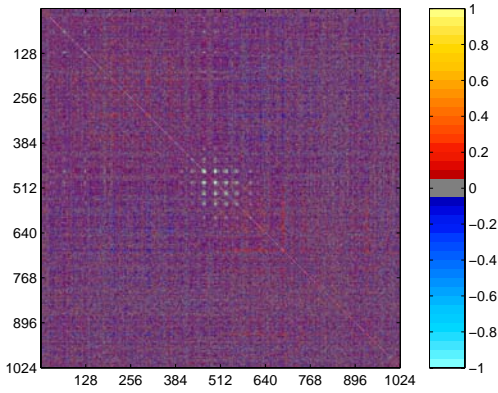
Figure 13: Correlation maps $p_y = p_x = 32$ $\rho = Real$, $n = 256$.



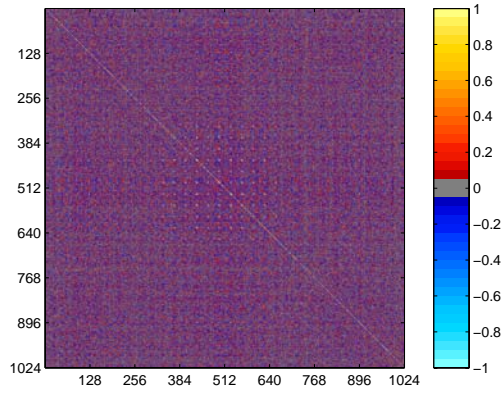
(a) $Corr(EPI(S_R), EPI(S_R))$



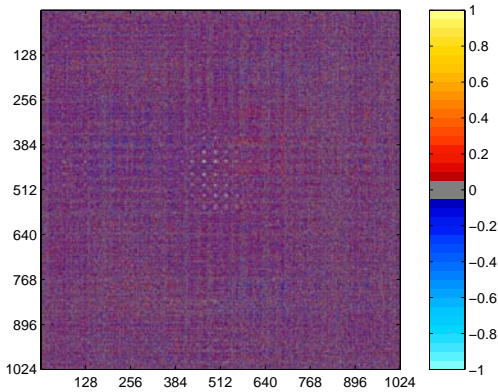
(b) $Corr(VEC(S_R), VEC(S_R))$



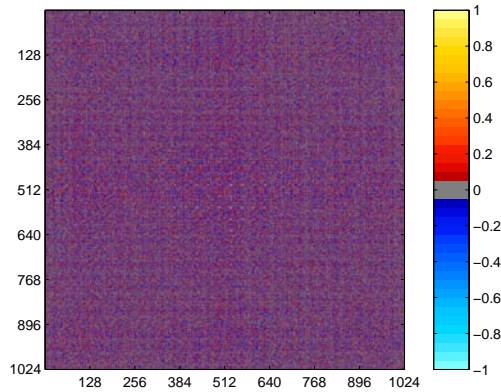
(c) $Corr(EPI(S_I), EPI(S_I))$



(d) $Corr(VEC(S_I), VEC(S_I))$

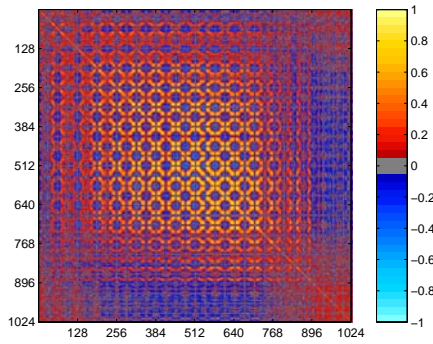


(e) $Corr(EPI(S_R), EPI(S_I))$

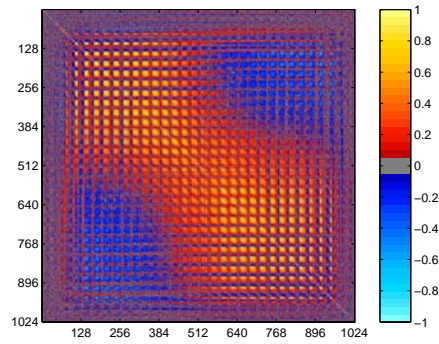


(f) $Corr(VEC(S_R), VEC(S_I))$

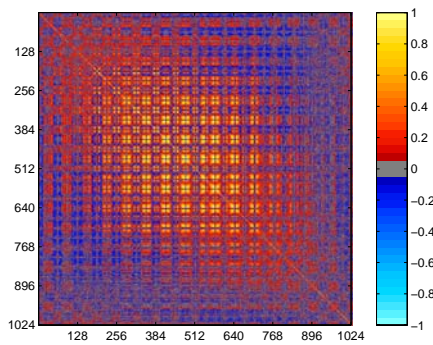
Figure 14: Correlation maps $p_y = p_x = 32$ $\rho = Real$, $n = 256$.



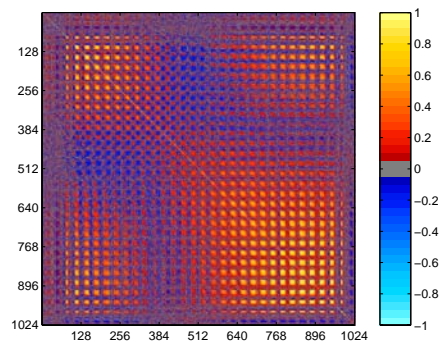
(a) $Corr(EPI(R_R), EPI(R_R))$



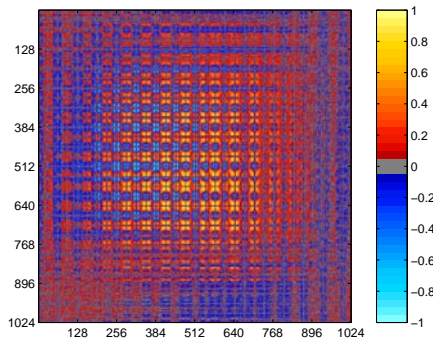
(b) $Corr(VEC(R_R), VEC(R_R))$



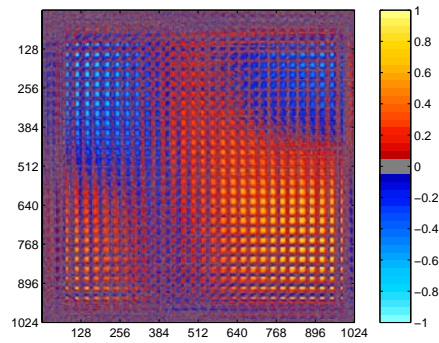
(c) $Corr(EPI(R_I), EPI(R_I))$



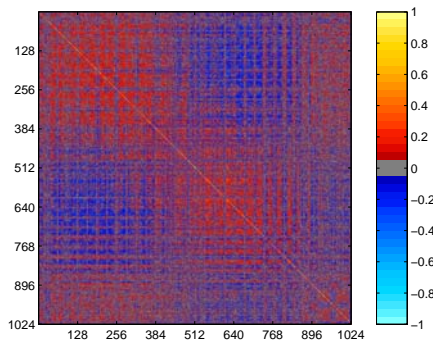
(d) $Corr(VEC(R_I), VEC(R_I))$



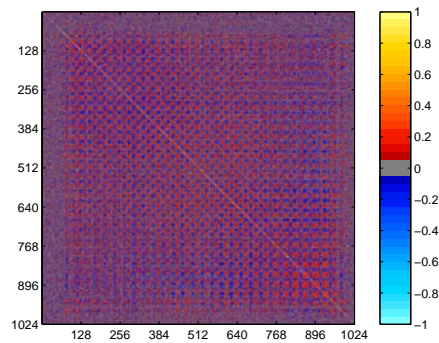
(e) $Corr(EPI(R_R), EPI(R_I))$



(f) $Corr(VEC(R_R), VEC(R_I))$

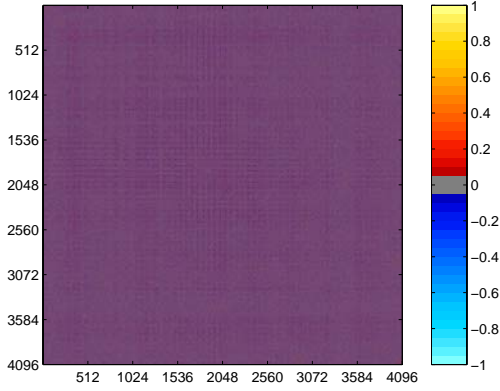


(g) $Corr(EPI(M), EPI(M))$

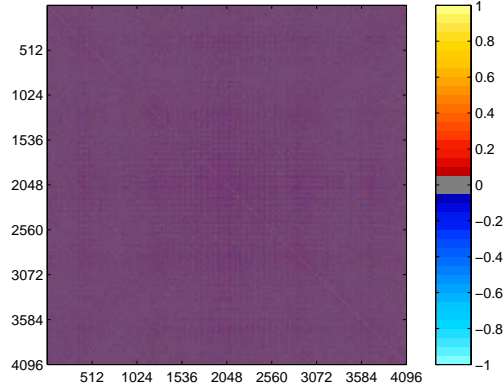


(h) $Corr(VEC(M), VEC(M))$

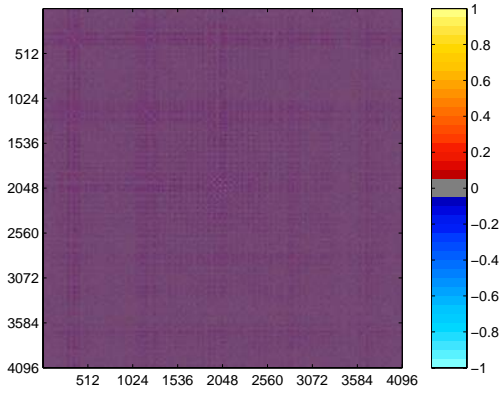
Figure 15: Correlation maps $p_y = p_x = 64$ $\rho = Real$, $n = 256$.



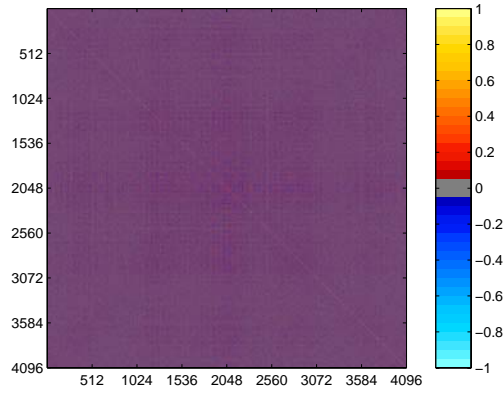
(a) $Corr(EPI(S_R), EPI(S_R))$



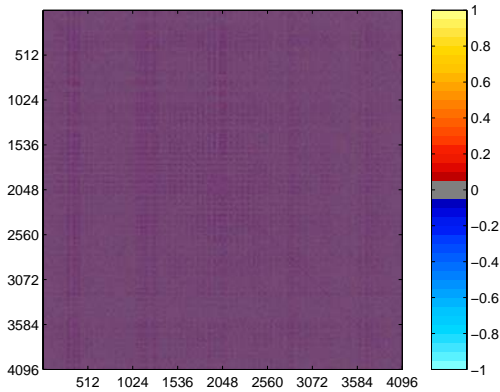
(b) $Corr(VEC(S_R), VEC(S_R))$



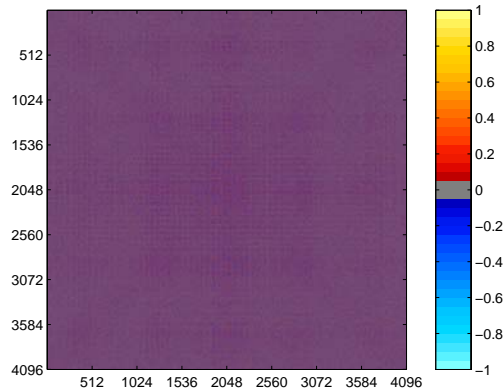
(c) $Corr(EPI(S_I), EPI(S_I))$



(d) $Corr(VEC(S_I), VEC(S_I))$

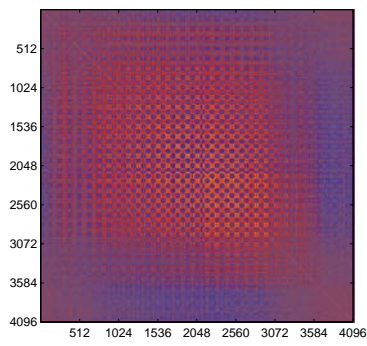


(e) $Corr(EPI(S_R), EPI(S_I))$

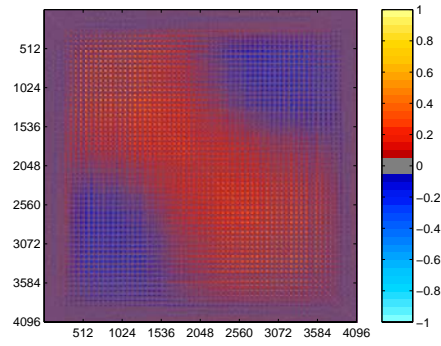


(f) $Corr(VEC(S_R), VEC(S_I))$

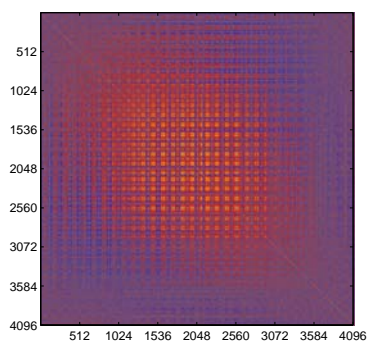
Figure 16: Correlation maps $p_y = p_x = 64$ $\rho = Real$, $n = 256$.



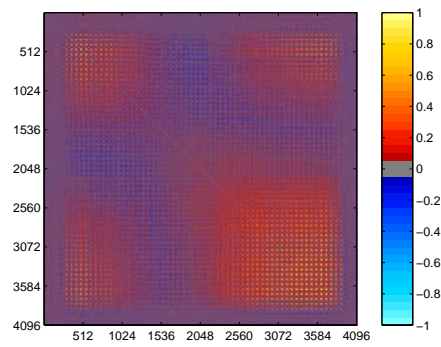
(a) $Corr(EPI(R_R), EPI(R_R))$



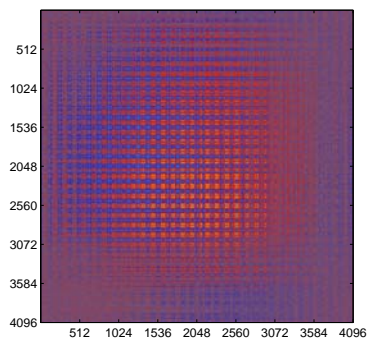
(b) $Corr(VEC(R_R), VEC(R_R))$



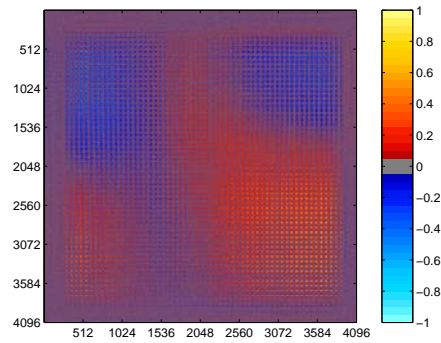
(c) $Corr(EPI(R_I), EPI(R_I))$



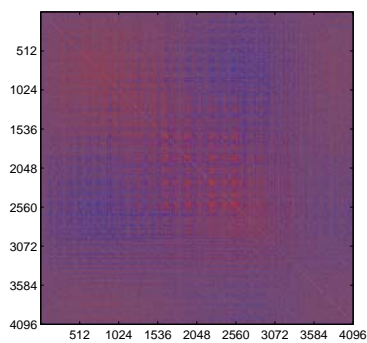
(d) $Corr(VEC(R_I), VEC(R_I))$



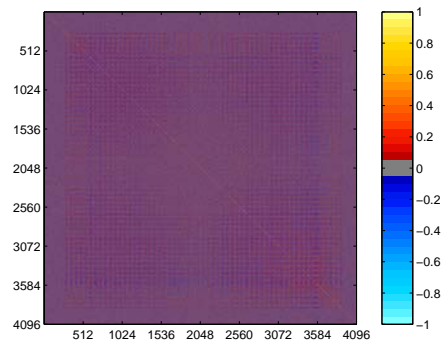
(e) $Corr(EPI(R_R), EPI(R_I))$



(f) $Corr(VEC(R_R), VEC(R_I))$



(g) $Corr(EPI(M), EPI(M))$



(h) $Corr(VEC(M), VEC(M))$

6 Conclusions

This paper examined the resulting correlation structure between voxels when Fourier reconstructing spatially correlated k -space observations. Spatially correlated voxels result from spatially correlated k -space observations. These correlation results may have implications for fMRI. In particular, temporally autocorrelated k -space measurements produce spatially correlated real and imaginary components of voxels along with the magnitude. This may have specific implications for functional connectivity. Further, the measurement process as implemented upon an aqueous phantom produced correlated voxels. The baseline spatial correlation needs to be considered and accounted for when making statements regarding connectivity between voxels in fMRI.

It is important to understand that the current fMRI noise process is not well understood for inanimate objects. Making statistical inferences, interpreting analysis results, and drawing conclusions should be drawn with the current research in mind.

Acknowledgements

The authors would like to thank Andrew Nencka for acquiring the phantom data. This work was supported in part by NIH R01EB00215, R01AG020279, and M01RR00058.

A Complex Normal Distribution

A complex-valued normal distribution was described by Wooding (1956) and further developments collected with additional applications by Anderson et al. (1995). Here the complex normal distribution as described by Anderson et al. (1995) is briefly summarized. However, this description departs from that of Anderson et al. (1995) in that the variance of the standard complex scalar variates is not renormalized to unity or equivalently that the variance of the standard real and imaginary variate parts of the scalar variates is not normalized to one-half.

Let $z_C = z_R + iz_I$ be a complex-valued scalar random variate where z_R and z_I are the real and imaginary variate parts of z_C . The complex variate z_C can be equivalently represented by the real-valued isomorphism $z = (z_R, z_I)'$. Let z_R and z_I be standard real normal scalar variates with mean zero and unit variance. Then utilizing the real isomorphism, z is bivariate normal with zero mean vector and identity two dimensional covariance matrix. The bivariate probability distribution function for real z is

$$p(z) = (2\pi)^{-\frac{2}{2}} |I_2|^{-\frac{1}{2}} e^{-\frac{1}{2} z'(I_2)^{-1} z}$$

where “ ’ ” denotes transposition and written $z \sim N(0, I_2)$. Returning to the complex representation, the probability distribution function for z_C is

$$p(z_C) = (2\pi)^{-\frac{2}{2}} e^{-\frac{1}{2} z_C^* z_C}$$

where “ * ” denotes conjugation and written $z_C \sim N_C(0, 1)$. A one-to-one correspondence between the probability function of the isomorphism z and the probability distribution function of z_C can readily be seen and that $z_C^* z_C \equiv z' z$ where “ \equiv ” denotes an equivalent relationship.

The nonstandardized complex scalar normal variate x_C can be found by pre multiplying z_C by $a_C = a_R + ia_I$ and adding $b_C = b_R + ib_I$. This transformation yields

$$\begin{aligned} x_C &= (a_R + ia_I)(z_R + iz_I) + (b_R + ib_I) \\ &= (a_R z_R - a_I z_I + b_R) + i(a_R z_I + a_I z_R + b_I) \\ &= x_R + ix_I . \end{aligned}$$

This transformation of the complex normal scalar variate can be represented in terms of the real isomorphism $x = az + b$ as

$$\begin{aligned} \begin{pmatrix} x_R \\ x_I \end{pmatrix} &= \begin{pmatrix} a_R & -a_I \\ a_I & a_R \end{pmatrix} \begin{pmatrix} z_R \\ z_I \end{pmatrix} + \begin{pmatrix} b_R \\ b_I \end{pmatrix} \\ &= \begin{pmatrix} a_R z_R - a_I z_I + b_R \\ a_R z_I + a_I z_R + b_I \end{pmatrix} \end{aligned} \tag{A.1}$$

with mean $\mu = 0 + b$

$$\mu = \begin{pmatrix} 0 \\ 0 \end{pmatrix} + \begin{pmatrix} b_R \\ b_I \end{pmatrix} \tag{A.2}$$

and covariance matrix

$$\begin{aligned}
aI_2a' &= \begin{pmatrix} a_R & -a_I \\ a_I & a_R \end{pmatrix} \begin{pmatrix} 1 & 0 \\ 0 & 1 \end{pmatrix} \begin{pmatrix} a_R & a_I \\ -a_I & a_R \end{pmatrix} \\
&= \begin{pmatrix} a_R^2 + a_I^2 & 0 \\ 0 & a_R^2 + a_I^2 \end{pmatrix}
\end{aligned} \tag{A.3}$$

where the variance is defined to be $\sigma^2 = a_R^2 + a_I^2$. The probability distribution function for this bivariate real isomorphism is

$$p(x) = (2\pi)^{-\frac{2}{2}} |\sigma^2 I_2|^{-\frac{1}{2}} e^{-\frac{1}{2}(x-\mu)'(\sigma^2 I_2)^{-1}(x-\mu)} .$$

Returning to the complex representation, the probability distribution function for nonstandard complex scalar normal variate x_C is

$$p(x_C) = (2\pi\sigma^2)^{-\frac{2}{2}} e^{-\frac{1}{2}(x_C - \mu_C)^*(\sigma^2)^{-1}\frac{1}{2}(x_C - \mu_C)}$$

and written $x_C \sim N_C(\mu_C, \sigma^2)$. Again, a one-to-one correspondence between the probability function of the isomorphism x and the probability distribution function of x_C can readily be seen and that $x_C^* x_C \equiv x'x$.

A multivariate or vector complex normal distribution can also be derived. Consider a collection of complex scalar normal variates x_{C1}, \dots, x_{Cp} or the equivalent real isomorphism x_1, \dots, x_p . Collect the real variates into a $p \times 2$ matrix $X = (x_1, \dots, x_p)'$ and form the $2p \times 1$ vector $x = \text{vec}(X)$ where $\text{vec}(\cdot)$ denotes the vectorization operator that stacks the columns of its matrix argument. The probability distribution function of x is

$$p(x) = (2\pi)^{-\frac{2p}{2}} |(\sigma^2 I_2) \otimes I_p|^{-\frac{1}{2}} e^{-\frac{1}{2}(x-\mu)'[(\sigma^2 I_2) \otimes I_p]^{-1}(x-\mu)} .$$

where \otimes denotes the Kronecker product and $\mu = \text{vec}(M)$ with $M = (\mu_1, \dots, \mu_p)'$.

The complex multivariate or vector normal distribution with correlation both within and between the real and imaginary parts can be derived via a transformation of variable. The nonstandardized complex p -dimensional multivariate normal variate y_C can be found by pre multiplying x_C by $A_C = A_R + iA_I$ and adding $d_C = d_R + id_I$. This transformation yields

$$\begin{aligned}
y_C &= (A_R + iA_I)(x_R + ix_I) + (d_R + id_I) \\
&= (A_R x_R - A_I x_I + d_R) + i(A_R x_I + A_I x_R + d_I) \\
&= y_R + iy_I .
\end{aligned}$$

This transformation of the complex normal vector variate can be represented in terms of the real isomorphism $y = Ax + d$ as

$$\begin{aligned}
\begin{pmatrix} y_R \\ y_I \end{pmatrix} &= \begin{pmatrix} A_R & -A_I \\ A_I & A_R \end{pmatrix} \begin{pmatrix} x_R \\ x_I \end{pmatrix} + \begin{pmatrix} d_R \\ d_I \end{pmatrix} \\
&= \begin{pmatrix} A_R x_R - A_I x_I + d_R \\ A_R x_I + A_I x_R + d_I \end{pmatrix}
\end{aligned} \tag{A.4}$$

with mean generically denoted as $\mu = b + d$ and covariance matrix $\Delta = A(\sigma^2 I_p)A'$ given by

$$\begin{aligned}
\Delta &= \begin{pmatrix} A_R & -A_I \\ A_I & A_R \end{pmatrix} \begin{pmatrix} \sigma^2 I_p & 0 \\ 0 & \sigma^2 I_p \end{pmatrix} \begin{pmatrix} A'_R & A'_I \\ -A'_I & A'_R \end{pmatrix} \\
&= \begin{pmatrix} A_R(\sigma^2 I_p)A'_R + A_I(\sigma^2 I_p)A'_I & -(A_I(\sigma^2 I_p)A'_R - A_R(\sigma^2 I_p)A'_I) \\ A_I(\sigma^2 I_p)A'_R - A_R(\sigma^2 I_p)A'_I & A_R(\sigma^2 I_p)A'_R + A_I(\sigma^2 I_p)A'_I \end{pmatrix} \\
&= \begin{pmatrix} \Sigma & -\Upsilon \\ \Upsilon & \Sigma \end{pmatrix}.
\end{aligned} \tag{A.5}$$

The probability distribution function for this multivariate real isomorphism is

$$p(y) = (2\pi)^{-\frac{2}{2}} |\Delta|^{-\frac{1}{2}} e^{-\frac{1}{2}(y-\mu)'\Delta^{-1}(y-\mu)}.$$

Returning to the complex representation, the probability distribution function for nonstandard complex scalar normal variate y_C is

$$p(y_C) = (2\pi)^{-\frac{2}{2}} |\Delta_C|^{-\frac{1}{2}} e^{-\frac{1}{2}(y_C-\mu_C)^H \Delta_C^{-1} (y_C-\mu_C)}$$

where “ H ” denotes the Hermitian or conjugate transpose, and is written $y_C \sim N_C(\mu_C, \Delta_C)$. Again, a one-to-one correspondence between the probability function of the isomorphism y and the probability distribution function of y_C can readily be seen and that $(y_C - \mu_C)^H \Delta_C^{-1} (y_C - \mu_C) \equiv (y - \mu)'\Delta^{-1}(y - \mu)$ where $\Delta_C = \Sigma + i\Upsilon$. To see this correspondence, note that

$$\Delta^{-1} = \begin{pmatrix} P & Q \\ -Q & P \end{pmatrix}$$

where $P = (\Sigma + \Upsilon\Sigma^{-1}\Upsilon)^{-1}$ and $Q = \Sigma^{-1}\Upsilon(\Sigma + \Upsilon\Sigma^{-1}\Upsilon)^{-1}$ along with $\Delta_C^{-1} = P - iQ$.

The complex matrix normal distribution of dimension $n \times p$ with correlation both within and between the real and imaginary parts can be derived via a transformation of variable. A set of p -dimensional complex-valued normally distributed random vectors y_{C1}, \dots, y_{Cq} that are mutually independent such that $y_{Cj} \sim N_C(\mu_{Cj}, \Delta_C)$, for $j = 1, \dots, q$ can be collected into a matrix $Y_C = (y_{C1}, \dots, y_{Cq})^H$. Then, Y_C , has a complex matrix normal distribution with mean and variance given by

$$\begin{aligned}
E(Y_C) &= (\mu_{C1}, \dots, \mu_{Cq})^H = M_C \\
var(Y_C) &= I_q \otimes \Delta_C.
\end{aligned}$$

This is denoted, $Y_C \sim N_C(M_C, I_q \otimes \Delta_C)$. The probability distribution function of Y_C is

$$p(Y_C) = (2\pi)^{-\frac{2pq}{2}} |\Delta_C|^{-q} e^{-tr[(Y_C - M_C)^H (Y_C - M_C) \Delta_C^{-1}]}$$

where tr denotes the trace operator.

This can be generalized to allow correlation between the rows of Y_C by the transformation of variable $U = D_C Y_C$

to form

$$\begin{aligned}
U_C &= (D_R + iD_I)(Y_R + iY_I) \\
&= (D_R Y_R - D_I Y_I) + i(D_R Y_I + D_I Y_R) \\
&= U_R + iU_I .
\end{aligned}$$

then the mean and variance given by

$$\begin{aligned}
E(U_C) &= D_C M_C \\
\text{var}(U_C) &= D_C D_C^H \otimes \Delta_C .
\end{aligned}$$

This is denoted, $U_C \sim N_C (D_C M_C, D_C D_C^H \otimes \Delta_C)$. The probability distribution function of U_C is

$$p(U_C) = (2\pi)^{-\frac{2pq}{2}} |\Delta_C|^{-q} |D_C D_C^H|^{-p} e^{-\text{tr}[(D_C D_C^H)(Y_C - M_C)^H (Y_C - M_C) \Delta_C^{-1}]}$$

References

- [1] H.H. Anderson, M. Højbjerg, D. Sørensen, and P.S. Eriksen. *Linear and Graphical Models for the Multivariate Complex Normal Distribution*. Springer-Verlag, New York, NY, USA, 1995.
- [2] P. Bandettini, A. Jesmanowicz, E. Wong, and J.S. Hyde. Processing strategies for time-course data sets in functional MRI of the human brain. *Magn. Reson. Med.*, 30(2):161–173, 1993.
- [3] F. Bloch. Nuclear induction. *Physical Review*, 70(7-8):460–474, 1946.
- [4] F. Bloch, W.W. Hansen, and M. Packard. The nuclear induction experiment. *Physical Review*, 70(7-8):460–474, 1946.
- [5] R.W. Cox, A. Jesmanowicz, and J.S. Hyde. Real-time functional magnetic resonance imaging. *Magn. Reson. Med.*, 33(2):230–236, 1995.
- [6] H. Gudbjartsson and S. Patz. The Rician distribution of noisy data. *Magn. Reson. Med.*, 34(6):910–914, 1995.
- [7] E.M. Haacke, R. Brown, M. Thompson, and R. Venkatesan. *Magnetic Resonance Imaging: Principles and Sequence Design*. John Wiley and Sons, New York, 1999.
- [8] A. Jesmanowicz, E.C. Wong, and J.S. Hyde. Phase correction for EPI using internal reference lines. *Proc. Soc. of Magn. Reson. Med.*, 1:1239, 1993.
- [9] A. Jesmanowicz, E.C. Wong, and J.S. Hyde. Self correcting EPI reconstruction algorithm. *Proc. Soc. of Magn. Reson. Med.*, 1:619, 1995.
- [10] B.R. Logan and D.B. Rowe. An evaluation of thresholding techniques in fMRI analysis. *NeuroImage*, 22(1):95–108, 2004.
- [11] S.O. Rice. Mathematical analysis of random noise. *Bell system Tech. J.*, 23:282, 1944. Reprinted by N. Wax, Selected papers on Noise and Stochastic Process, Dover Publication, 1954. QA273W3.
- [12] D.B. Rowe. *Multivariate Bayesian Statistics*. CRC Press, Boca Raton, FL, USA, 2003.
- [13] D.B. Rowe. Modeling both the magnitude and phase of complex-valued fMRI data. *NeuroImage*, 25(4):1310–1324, 2005.
- [14] D.B. Rowe. Parameter estimation in the magnitude-only and complex-valued fMRI data models. *NeuroImage*, 25(4):1124–1132, 2005.
- [15] D.B. Rowe and B.R. Logan. A complex way to compute fMRI activation. *NeuroImage*, 23(3):1078–1092, 2004.
- [16] D.B. Rowe and B.R. Logan. Complex fMRI analysis with unrestricted phase is equivalent to a magnitude-only model. *NeuroImage*, 24(2):603–606, 2005.

- [17] G. Strang. *Linear Algebra and its Applications*. Harcourt Brace Jovanovich, Orlando, Florida, third edition, 1988.
- [18] R.A. Wooding. The multivariate distribution of complex normal variables. *Biometrika*, 43:212–215, 1956.